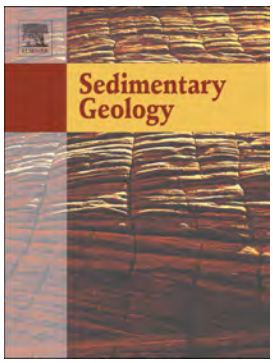

Periodicity in stromatolitic lamination: A potential record of ENSO, NAO, and SUNSPOT in the Miocene lacustrine record of the Ebro Basin, Spain

Francisco Javier Pérez-Rivarés, Leticia Martin-Bello, Concha Arenas-Abad

PII: S0037-0738(19)30147-2
DOI: https://doi.org/10.1016/j.sedgeo.2019.07.005
Reference: SEDGEO 5513

To appear in: *Sedimentary Geology*

Received date: 19 February 2019
Revised date: 15 July 2019
Accepted date: 17 July 2019

Please cite this article as: F.J. Pérez-Rivarés, L. Martin-Bello and C. Arenas-Abad, Periodicity in stromatolitic lamination: A potential record of ENSO, NAO, and SUNSPOT in the Miocene lacustrine record of the Ebro Basin, Spain, Sedimentary Geology, https://doi.org/10.1016/j.sedgeo.2019.07.005

Periodicity in stromatolitic lamination: a potential record of ENSO, NAO, and SUNSPOT in the Miocene lacustrine record of the Ebro Basin, Spain

Francisco Javier Pérez-Rivarés[a], Leticia Martin-Bello[a,b], Concha Arenas-Abad[a,b]

[a]Department of Earth Sciences, University of Zaragoza. 50009 Zaragoza, Spain

[b]Institute for Research on Environmental Sciences of Aragón (IUCA) and Geotransfer group. University of Zaragoza. 50009 Zaragoza, Spain

*Corresponding author: Email. perezrivares@gmail.com

Abstract

The spectral decomposition of time series obtained from ancient rock records can be used to study the similarity between the dynamics of present-day and past climate systems. A high-resolution periodicity analysis of luminance and lamina thickness of lacustrine stromatolites in the Ebro Basin (northeast of Iberian Peninsula) reveals a significant signal of interannual and decadal climatic variability in the Miocene. This is one out of very few works that presents the use of spectral analysis to estimate the potential of stromatolite lamination as multiple-scale recorders of climate parameters. The effects of precipitation and evaporation variations on stromatolite lamination have been detected at three orders of cyclicity based on textural and high-resolution stable-isotope analyses (C and O) obtained in prior studies. These analyses also revealed that the light and dark simple lamina couplets are identified with annual cycles (third-

order isotopic cycles). In the present study, the spectral analysis results obtained through different paths in five stromatolite specimens reveal significant periods in the power spectrum at around 2.5, 3.7, 5, 7, 10, and 22 years. These cycles can be correlated with the typical oscillation bands of different climate-related agents. The 2.5-year period corresponds to the Quasi Biennial Oscillation (QBO), or to the biennial component of the El Niño-Southern Oscillation (ENSO), or to the North Atlantic Oscillation (NAO). The 3 to 5 and 5 to 7-year bands can be linked to ENSO or NAO variability (second-order isotopic cycles). The 8 to 11-year bands fit the 11-year Schwabe (first-order isotopic cycles) and 22 to 23-year fit the 22-year Hale sunspot cycles. Thus, the stromatolite growth was controlled by ENSO, NAO, and solar activity cycles. The close relationship between these climate-related agents makes it difficult to specify the dominant agent controlling the stromatolite growth. Nevertheless, the significant periods obtained from this study, within interannual (2.5, 3.7, 5, 7 years), decadal (10, 22 years), and even multidecadal bands (37-42 years), support the existence, and concurrence, of ENSO and NAO precursors during the early and middle Miocene.

Key words: lacustrine stromatolites; saline carbonates; annual lamina couplets; lamination periodicity; quasi-periodic cycles; Solar and calendar frequencies.

1. Introduction

The temporal significance of stromatolite lamination has been an intriguing, unsolved issue ever since its discovery. The difficulty in knowing the environmental significance of lamination comes from the wide variety of parameters that are involved in lamination development, and the several ranks of lamina arrangement (Hofmann, 1973; Petryshyn et al., 2012; Arenas and Jones, 2017). Most studies of stromatolite lamination are based on textural variations of the laminae, in some cases coupled with stable isotope analyses (C and O), which together provide palaeoclimatic and palaeoenvironmental information (Andrews and Brasier, 2005; Nehza et al.,

2009; Brasier et al., 2010; Osácar et al., 2013; Arenas et al., 2019). The stable isotope composition mainly yields information about temperature variations (Matsuoka et al., 2001; Kano et al., 2007; Brasier et al., 2010) or precipitation/evaporation conditions (Leng and Marshall, 2004; Arp et al., 2005; López-Blanco et al., 2016). The cyclic evolution of textural and stable isotope data, mostly $\delta^{18}O$, contribute to the inference of seasonal climatic changes (Kano et al., 2003, 2007; Dabkowski et al., 2015; Martin-Bello et al., 2019a). Clumped isotopes are a promising tool for obtaining temperature data from ancient stromatolites (e.g., Frantz et al., 2014; Kele et al., 2015; Kato et al., 2019). This technique is useful for inferring cyclic changes through time, from which durations can be inferred. However, its use is still limited, pending refinement of the equilibrium calculations (Affeck, 2012). Another way to estimate the temporal meaning of lamination is the study of modern stromatolites, through the periodic monitoring of deposition and the corresponding hydrological, climatic, sedimentary, and geochemical conditions (e.g., Kano et al., 2007; Gradziński, 2010; Arenas et al., 2014). These studies have mostly been performed in the fluvial environment, and show that a number of laminae can be formed annually or even seasonally (Manzo et al., 2012; Arenas and Jones, 2017).

Concurrent cyclic variations of textural and stable isotope composition in microbial lamination have been reported by several authors (e.g., Arp et al., 2010; Brasier et al., 2010; Dabkowski et al., 2015; Rodríguez-Berriguete et al., 2018; Martin-Bello et al. 2019a). These authors propose seasonal changes in climate parameters to explain such cyclic variations. In other cases, cyclicities based on lamina thickness, geochemical data or stable isotope data have also been related to climatic phenomena such as the El Niño-Southern Oscillation (ENSO) or SUNSPOT cycles (Mischke and Zhang, 2008; Tang et al., 2014; Petryshyn et al., 2015).

Despite inferences from textural and stable isotope composition in the ancient record, and comparisons with the recent record, the main problem in interpreting the temporal

significance of stromatolitic lamination comes from its fractal nature, which produces multiple ranks of laminae and of lamina arrangement (Monty, 1967; Nehza et al., 2009; Martin-Bello et al., 2019a). The spectral analysis of time series can help understand climate dynamics reflected in the geological record at different scales (e.g., Weddon, 1993 and references therein; Bond et al., 1997; Holmgren et al., 1999). This type of analysis has been applied to varied laminated ancient records in order to infer annual to multidecadal periodicity similar to the North Atlantic Oscillation (NAO) or ENSO variations (e.g., Huber and Caballero, 2003; Galeotti et al., 2010; Lenz et al., 2010; Batenburg et al., 2011; Walliser et al., 2017). The stable isotope variations in speleothem laminae from northern Italy, and in high-resolution lacustrine laminae from north-eastern Spain, have been suggested to have been significantly influenced by the NAO during the Holocene (Scholz et al., 2012; Muñoz et al., 2015). Other studies have associated the variations registered through the upper Miocene with the NAO or ENSO-like phenomena, as in the case of $\delta^{18}O$ records of corals of the Mediterranean (Brachert et al., 2006; Mertz-Kraus et al., 2009), and others from Pliocene lacustrine laminated sediments in Spain and Greece (Muñoz et al., 2002b; Kloosterboer-Van Hoeve et al., 2006). The periodicity of thickness values in upper Miocene halo-varves in Italy has also been related to the influence of ENSO variability (Galeotti et al., 2010). Even in the middle Oligocene, Walliser et al. (2017) have found that data on shell growth rates from long-lived marine bivalves in northern Europe yield variability comparable to that of the NAO. However, lacustrine stromatolites have not been explored yet in detail with such a periodic perspective by using spectral analysis.

The characterisation of atmospheric circulation phenomena and solar activity (as SUNSPOT phenomenon) as climate forcing agents is an important subject of study today. Additionally, several works have focussed on revealing the evidence of periodic or quasi-periodic behaviour of present-day climatic phenomena in records of the past. The persistence of these climatic phenomena over long time periods can help evaluate the predictability of the climatic conditions.

The purposes of this paper are: 1) to demonstrate the occurrence of different orders of periodicity of stromatolitic lamination; 2) to propose plausible temporal intervals for such orders; and 3) to suggest natural causes of such periodic changes, such as atmospheric circulation phenomena and solar activity. The study is based on the analysis of periodicity of time series built from discrete and continuous parameters of the laminae (e.g., luminance and thickness) obtained in several stromatolite specimens from the Miocene lacustrine record in the Ebro Basin, Spain. The results, supported by stable isotope analyses of previous works, provide new data on the temporal significance of stromatolitic lamination, and show the complexity of stromatolitic lamination and its potential to record multi-scale climate signatures, such as ENSO, NAO, and SUNSPOT variations. Moreover, this work contributes to knowledge on the influence of circulation patterns such as the NAO and ENSO on the climate of Europe, both in the past and at present.

2. Circulation phenomena and climate variability in present and Cenozoic environments

The solar activity that interacts with the Earth's surface is the sum of several processes that occur mainly in the convection zones, the photosphere, and the atmosphere of the Sun (Gray et al., 2010). Several Sun/Earth interaction mechanisms have been suggested in studies of the variability of solar activity influence on the Earth's climate system (Beer et al., 2000; Reid, 2000). It has been suggested that there is a relation between solar activity and ENSO variability (Hathaway, 2015; Zhai, 2017). Moreover, the spatial structure of the NAO in winter is significantly forced by the solar cycle (Kodera and Kuroda, 2005). Actually, the influence of solar activity on phenomena such as the NAO, ENSO, and AMO (Atlantic Multidecadal Oscillation) has been noted over the Atlantic/European sector (Gray et al., 2016).

Changes in rainfall and temperatures in northern and southern Europe are related to NAO

variability (Hurrell, 1995; Hurrell and van Loon, 1997; Jones et al., 2003). The more coherent variations occur on periods of 2.5, 5-6, and 8 years (Pozo-Vázquez et al., 2000; Weddon, 2003). It is considered that the phenomenon of mixed oceanic and atmospheric circulation known as ENSO is the globally dominant mode of interannual climate variability, and that it has a global influence over weather and climate. The influence of the ENSO on climate has also been studied in Europe (e.g., Vicente-Serrano, 2005; Brönnimann et al., 2007; Shaman and Tziperman, 2011; Kalimeris et al., 2017). The impact of the extreme phases of the ENSO on seasonal precipitation has also been detected on the Iberian Peninsula (Rodó et al., 1997; Rocha, 1999; Vicente-Serrano, 2005). Likewise, the association of NAO variability and rainfall on the Iberian Peninsula and in northern Africa has been the subject of various studies (Zorita et al., 1992; Rodó et al., 1997; Knippertz et al., 2003). The correlation found between the values of NAO indices and rainfall also applies to some places in the current Ebro Depression (Goodess and Jones, 2002; Muñoz-Díaz and Rodrigo, 2004; Hernández-Ballarín and Peláez-Campomanes, 2017). Present-day lakes are widely affected by climate variables, such as air temperature, wind velocity and precipitation (Margalef, 1983), and observations have demonstrated that many physical and biological lake properties are controlled by these parameters on seasonal to decadal scales (Catalan et al., 2013). Likewise, the NAO produces a pronounced effect on the physics, chemistry, and biology of many northern hemisphere lakes and rivers (Straile et al., 2003). The NAO exerts a dominant influence on European lakes in winter and early spring, when spring turnover and the onset of stratification occur, but the influence is noted through the year. Thus, the NAO exerts a major impact on the seasonal distribution of temperature and nutrients (Hurrell et al., 2003; Straile et al., 2003). Similarly, the relation between interannual variations of lake level and river discharge in Africa and Asia are shown to be mainly driven by precipitation changes that are associated with the ENSO (Mercier et al., 2002; Hwang et al., 2005; Okonkwo et al., 2014). In Europe, surface pressure, temperature and precipitation data collected from several studies reveal ENSO influence on

lake water features (Fraedrich and Muller, 1992). Climatic sensors from a modern saline lake in the south of the Sierra de Alcubierre also manifest positive response of lake level variations to ENSO parameters, such as precipitation (Rodó et al. 1997).

Thus, numerous studies support the influence, at present-day, of the phenomena of circulation such as ENSO and NAO on the seasonal distribution of temperature and rainfall of Europe and specifically of the Iberian Peninsula. Likewise, several works support the idea that periodicity oscillations found in the ancient record can also be attributed to ENSO effects (Mingram, 1998; Galeotti et al., 2010; Lenz et al., 2010). In this line of argument, Mingram (1998) indicated the presence of a 5.5 yr periodicity in Eocene laminated lacustrine deposits of central Europe (Germany). Similarly, Lenz et al. (2010) found that, during the cold interval of the Eocene, lacustrine laminated oil shales in Central Europe showed thickness variability attributable to ENSO effects. In contrast, other works consider that these periodic or quasi-periodic variations could have been produced by NAO effects (Brachert et al., 2006; Mertz-Kraus et al., 2009; Walliser et al., 2017). Both Brachert et al. (2006) and Walliser et al. (2017) provided information on numerical climate models and distribution of wSLP-EOF (winter Sea-Level Pressure-Empirical Orthogonal Function) domains in the North Atlantic ocean that led them to propose the NAO, and not ENSO, as the main cause of the seasonal and interannual climate variability recorded through the growth of corals and bivalves. Walliser et al. (2017) did not discard the hypothesis that both circulation patterns (NAO and ENSO) could coexist in the Oligocene and Miocene, as it happens nowadays.

During the late Miocene, it has been recognised that climate conditions allowed sea surface temperature (SST) gradients similar to those that cause the El Niño phenomenon at present (Holbourn et al., 2018). In the western Pacific, during the Miocene, there was a substantial interannual variability of SST, with a 3-year periodicity (Batenburg et al., 2011). Variations in $\delta^{18}O$ records of corals of the late Miocene Mediterranean have been associated with variations

in SST and the hydrologic balance of sea water, both influencing sea surface salinity. All these parameters have an interannual variability with periods linked to the NAO or ENSO-like phenomena (Brachert et al., 2006; Mertz-Kraus et al., 2009). The periodicity of thickness values of late Miocene halo-varves in Italy has been related to variation in SST influenced by ENSO variability (Galeotti et al., 2010). In the Iberian Peninsula, the regional palaeogeographic configuration during the Miocene would be similar to the present one (Bice et al., 2000; Seton et al., 2012; Scotese, 2014) and therefore could provide suitable conditions for these phenomena to occur.

3. Geological setting

The Ebro Basin is located in the northeastern sector of the Iberian Peninsula and is bounded by the Pyrenean, Iberian, and Catalonian Coastal ranges (Fig. 1A). It is the latest southern foreland basin of the Pyrenean orogen (Riba et al., 1983). The basin fill comprises marine and non-marine deposits from Palaeocene to late Eocene times. From the latest Eocene (Costa et al., 2010), the basin became fully continental. Then, it was filled with alluvial and fluvial sediments derived from the rising bounding ranges, and evaporite and carbonate deposits in lacustrine systems in the basin centre.

The Ebro Basin fill has been divided into eight genetic stratigraphic units, denominated tectosedimentary units (T1 to T8; Muñoz et al., 2002a; Pardo et al., 2004). Units T1 to T3 were deposited up to the upper Oligocene; unit T4 is Oligocene to lower Miocene in age, and units T5 to T8 are Miocene in age. In the middle or late Miocene the basin opened to the Mediterranean sea (Arche et al., 2010; Vázquez-Urbez et al., 2013), starting an emptying phase that continues to the present day. As a consequence of the extensive erosion during the Pliocene and Quaternary, several uplands formed in the central part of the basin. One of those uplands is the Sierra de Alcubierre, which is the study area of this research.

The Sierra de Alcubierre area comprises *ca* 600 m of lacustrine and distal fluvial deposits. In the area there are no active tectonic structures and the strata are close to horizontal, dipping slightly to the south-southwest. The succession is divided into three tectosedimentary units: T5, T6 and T7 (Fig. 1B), which span from the Agenian to the Aragonian (equivalent to the Aquitanian and Serravalian, respectively) (Muñoz et al., 2002a). These units have been dated by magnetostratigraphy as 21.3 to 13.5 Ma (Fig. 1C)(Pérez-Rivarés et al., 2002, 2018). Unit T5 (approximately 4.6 Ma) is formed of 430 m of mudstone, sandstone, gypsum, marl, limestone, and dolostone strata, which grade laterally into limestone and marl deposits to the east and north (Fig. 1C). Further north, these lacustrine deposits pass laterally into fluvial mudstones and sandstones. Unit T6 (approximately 1.9 Ma) includes 135 m of mainly limestone and marl deposits; gypsum strata are interbedded toward the southwestern part of the Sierra (Fig. 1C). Unit T7 (approximately 1 Ma) comprises 110 m of mudstone, sandstone, limestone, and marlstone strata. The stromatolites are associated with laminated limestones in the three units, being more common and thicker in units T5 and T6 (Fig. 1B, 1C) (Arenas et al., 1997).

Arenas and Pardo (1999) proposed a lacustrine facies model for units T5 and T6 in the central sector of Ebro Basin, including the Sierra de Alcubierre, during the Miocene. The depositional model is defined by lake level fluctuations. During high lake levels freshwater carbonate conditions promoted massive and bioturbated limestone and marl facies formation. Low lake levels led to sulphate and halite facies development in a playa-lake system. Stromatolites and laminated limestones and dolostones developed at intermediate lake level settings, i.e., during oscillations between high and low lake levels that yielded saline carbonate conditions. These oscillations are related to climatic variations. Indeed, the lacustrine record of the Sierra de Alcubierre has been shown to reflect the influence of astronomic climatic signatures (Pérez Rivarés, 2016). Cyclostratigraphic analysis of some Miocene lacustrine sections showed that decimetre to decametre-scale sequences could be linked to Milankovitch frequencies. Correlation between local magnetostratigraphy (Pérez Rivarés, 2016) and Laskar solutions

(Laskar et al., 2004) has allowed the matching of groups of marl-limestone couplets with astronomical precession (23-kyr), and short (100-kyr), large (400-kyr), and very large (1.2-Myr) eccentricity cycles (Pérez Rivarés, 2016).

Within the context of saline carbonate conditions, in the study area, three types of stromatolites have been distinguished: thin planar, stratiform and domed. Thin planar stromatolites have greater length than height (up to 6 m long and up to 10 cm thick). They usually have flat-to-undulatory, laterally continuous laminae, and developed in shallow and marginal lake areas prone to subaerial exposure. Stratiform stromatolites are 10 to 30 cm thick and 10 to 30 m long, and include varied internal growth forms (columns, domes and undulatory to flat-laminated forms). Domed stromatolites are 10 to 30 cm thick and of similar length. They are formed of similar internal growth forms to those in the stratiform stromatolites. Stratiform and domed stromatolites are related laterally (Martin-Bello et al., 2019b). The three types of stromatolites are composed of different lamina types and lamina arrangements.

4. Materials and methods

Five specimens of lacustrine stromatolites from the Sierra de Alcubierre (Fig. 2; PL-22, VS-22, AC-5, SC-6, and SC-141) were collected from units T5 and T6 (locations and horizons in Fig. 1B, 1C). The specimens are 4–12 cm thick. High-resolution images (1000 ppi) were obtained directly through digital scanning of polished sections across the lamination. Lamina thickness and luminance values were used to analyse the cyclicity registered by the stromatolitic laminae. Both types of data were measured using the multipurpose software for stratigraphic signal analysis Strati-Signal (Ndiaye et al., 2012). In order to measure these values, several paths perpendicular to the lamination were selected on the images of the specimens (Fig. 2). Due to the morphology of the laminae (see Fig. 3A) and to avoid artefacts or defects, running

several segments was necessary to cover the whole specimen. In specimens PL-22, VS-22, and SC-6 the spectral analysis was performed following two paths across the specimens (Fig. 2). Path-A was conducted across portions of the specimen with flat laminae, while Path-B was performed across portions with more convex laminae (or through summit portions in specimen SC-6; Fig. 2). Each path shows dissimilar variations of lamina thickness. Data obtained from the time-equivalent interval of the two paths in each of the three specimens were used to evaluate the coherence of the cyclicity results.

Rock colour records were extracted from digital images of scanned stromatolite surfaces in the CIE-L*ab colour space. Each value resulted from the average of eight laterally aligned measurements, obtained by a maximum luminance pixel integration window (imperfections were usually revealed as darker pixels). Successive values were plotted along the segments normal to the laminae. These data points were used to construct luminance curves for each path. A linear de-trending was applied to the data.

A semi-automated lamina counting was implemented in order to give a class (dark or light) to each type of lamina and then calculate its thickness. The light class includes both light dense micrite laminae and light porous micrite to microsparite laminae. The dark class is identified with dark dense micrite laminae. This type of grouping is also based on the isotopic values of the laminae (Martin-Bello et al., 2019b). For the classification process, a moving average data smoothing was applied to the luminance curves. The width of the smoothing window was specified as 15 data. A last value padding of the data was applied to avoid the loss of sample size due to the moving average application. The original luminance and the smoothed-luminance curves have been overlaid to have a Boolean discriminatory condition: a datum of the original luminance curve is classified as light lamina class if its luminance value is higher than the homologous value of the smoothed luminance curve, and as dark lamina class if it is lower. Other classification methods were tested, such as fuzzy logic and instance-based

learning (Dasarathy, 1991), but the results were less discriminatory (with overestimation of dark laminae), presumably due to the high presence of imperfections and the higher variability of luminance of the light laminae compared to the dark ones. The output classes were then compared with visual representations of the stromatolitic laminations, and the discrepancies in automatic classification manually corrected. Thus, it was possible to obtain the thickness measurements of the stromatolite laminae. Subsequently, several time series were elaborated based on: raw luminance data, the thicknesses of simple light and simple dark laminae, and the sum of thicknesses of the light and dark laminae (light-dark lamina couplets)(Supplementary material 1).

The time series were analysed to reveal periodic cycles in lamina thickness using the Fourier transform and wavelet spectral method, with the spectral analysis programme REDFIT (Schulz and Mudelsee, 2002), and Wavelet analysis (Torrence and Compo, 1998) integrated in the software PAST (PAleontological STatistics V. 2.15; Hammer et al., 2001). REDFIT automatically removes the trend by subtracting the mean prior to time series analyses.

To distinguish the frequency cycles (spectral peaks) from background variability, the time series were tested against red noise. As greater amplitude values at low frequencies are a characteristic of climate time series (e.g., Weddon, 2003; Ólafsdóttir et al., 2013), the implementation of this type of error is adequate. A first-order autoregressive (AR(1)) process (i.e., red noise) was applied to form a theoretical red noise spectrum and false-alarm at 90, 95, and 99% levels (Thomson, 1990).

Moreover, in order to reveal variations in the spectral profiles through time (following the stromatolite lamina accretion), wavelet spectral analyses were performed. The Morlet wavelet base (wavenumber 6) was used, which is the most commonly used wavelet in geophysics (Lau and Weng, 1995). The temporal series were padded with zeros at both ends, to limit the edge effect. A cone of influence was included to indicate the region of the wavelet spectrum where

the results were less reliable. Background noise was an autoregressive model AR(1), and the statistical significance of the wavelet power spectrum was evaluated with a 5% significance level (95% confidence threshold).

5. Stromatolite lamination

Textural, structural, and stable-isotopic data for the studied stromatolite deposits are discussed in Martin-Bello et al. (2019a, 2019b). This paper provides only contextual information to help interpret the lamina cyclicity data within the lacustrine environment and the results derived from the periodicity data obtained herein.

5.1 Characteristics of the laminae and lamination

The studied stromatolites are formed of micrite and microsparite laminae, with occasional fibrous laminae (i.e., they are fine-grained or micritic stromatolites, *sensu* Riding, 2000). They consist of calcite, with variable amounts of dolomite in some specimens. The laminae are laterally continuous, with variable thicknesses and cross-sectional shapes. They vary from flat to gently to steeply convex (Fig. 3A).

Four types of simple laminae (i.e., smallest units of uniform texture, cf. Arenas and Jones, 2017) have been defined by their texture, colour, and porosity (Martin-Bello et al., 2019b). Three of them compose the stromatolites used for this study and are described below (Fig. 3B):

- Dark dense micrite laminae (0.04 – 0.5 mm thick) are composed of dark grey micrite. These laminae are laterally continuous, with uniform thickness. Elongated pores (40 µm) parallel to the lamination are occasionally present.

- Light porous micrite to microsparite laminae (0.08 – 1.3 mm thick) are formed mainly of light grey to brown porous micrite, typically forming micropeloidal fabrics. The thickness varies

laterally, decreasing down the sides of the domes, sometimes disappearing, and increasing at the summit of the domes.

- Light dense micrite laminae (0.1 – 1.9 mm thick) are composed of light grey to light brown micrite, and include scattered small quartz grains, bioclasts, intraclasts, and ooids. The thickness varies laterally in an irregular way.

The boundaries between simple laminae are consistent in all the stromatolites: gradual from light dense laminae to light porous laminae, and gradual or sharp from light laminae to dark dense laminae, but the boundaries at the top of the dark dense laminae are always sharp.

In polished sections, the dark dense laminae are distinguished as dark yellow to brown laminae, while the light dense laminae and light porous laminae are light yellow, white or cream in colour (Fig. 3D).

Several simple laminae can be grouped into composite laminae in which either the dark or the light laminae are dominant (Fig. 3B). Dark composite laminae (0.2 – 2.8 mm thick) are characterised by dark dense micrite laminae with thin light porous lamina intercalations, or by the succession of dark dense micrite laminae (Fig. 3B, 3C). Light composite laminae (0.6 – 6.4 mm thick) show light porous laminae with thin dark dense lamina intercalations, or alternating light porous and light dense laminae (Fig. 3B, 3C).

Overall, in the studied rocks, post-sedimentary features at the scale of microfacies consist of microspar and spar calcite cements, either in intergranular or framework or rare moldic porosity. Dissolution and replacement features are not common. In the studied stromatolites the contacts between the several lamina ranges are either gradual or sharp and coincide with changes in crystal size and/or porosity; the boundaries between laminae are not found within crystals nor within crystalline bands, as described in other laminated carbonates (Rodríguez-Berriguete et al., 2018). Moreover, the stable isotope composition from high-resolution

sampling of a specimen parallels textural changes and colour variations. Together these features indicate that diagenesis did not influence significantly the lamina boundaries, and thus the measurement of thickness based on colour can be considered close to pristine.

5.2 Stable isotope composition

Previous studies of the Miocene lacustrine stromatolites in the Ebro Basin, based on textural and stable isotopic analyses ($\delta^{13}C$ and $\delta^{18}O$) suggested that changes in the precipitation/evaporation ratio (P/E) were the main factor controlling the cyclic variations between light (either porous or dense laminae) and dark dense laminae (Martin-Bello et al., 2019a, 2019b). Temperature effects are less clearly reflected in the isotopic record of closed lacustrine basins (Kelts and Talbot, 1990; Leng and Marshal, 2004; Arp, et al., 2005; López-Blanco et al., 2016), such as the Ebro Basin in the lower and middle Miocene. Accordingly, the light laminae, with lower isotopic C and O values, correspond to more humid conditions, while the dark laminae, with higher isotopic C and O values, developed under drier conditions (Martin-Bello et al., 2019a, 2019b). The authors assumed that the higher temperatures would be related to drier periods, while the cooler temperatures would be related to more humid conditions, as is nowadays (the latitude of the studied area was similar today and in the Miocene). Martin-Bello et al. (2019a), through a High Resolution Sampling study, detected three orders of cyclicity in the isotopic variations of both $\delta^{13}C$ and $\delta^{18}O$, which were related to P/E changes reflected in textural changes. First order isotopic cycles correspond to couplets formed of a light composite lamina followed by a dark composite lamina; this succession was interpreted as representing an overall decrease in the P/E ratio (Fig. 4B). Second order isotopic cycles correspond to each composite dark or each composite light lamina, which are thought to represent periods of drier or more humid climatic conditions, respectively. The highest frequency order cycles (third order) are the light-dark simple lamina couplets, each couple reflecting seasonal P/E ratio variations through a year. According to these premises, the dark

dense simple laminae were interpreted to have developed mostly in summer, and the light porous and light dense simple laminae during the cool seasons (Kano et al., 2003; Martin-Bello et al., 2019a). Textural features allow to infer that the light porous simple laminae would have formed during the spring to early summer periods, and the light dense simple laminae during the autumn to early spring (Fig. 5). The succession of the three types of simple laminae, and the stable isotopic composition of the light versus dark laminae, allowed the authors to suggest that each light-dark simple lamina couplet represents one year.

6. Results

6.1. Stromatolite growth rates

Assuming that each light-dark lamina couplet represents a year of growth of the stromatolites of the Sierra de Alcubierre, the stromatolite records studied here span between 120 and 500 years. An average growth rate of the studied Miocene stromatolites of 0.362 mm yr^{-1} can be calculated (between 0.199 and 0.540 mm yr^{-1}; Table 1). Table 1 shows a remarkable difference between the rates observed in unit T5 (0.21 mm yr^{-1}) and unit T6 (0.41 mm yr^{-1}); however this difference is mainly due to the type of morphology of the laminae (flat or domed; Path- A or -B) and therefore there is no relation with the unit in which they occur.

6.2 Description of the cyclicity of stromatolite lamination

Thickness and colour variations of the laminae can be recognised on polished sections on different scales, i.e. forming cycles of different orders. Specimens PL-22, VS-22, and SC-6 show clear variations that can be associated with cyclic patterns. Three order cycles have been recognised by manual counting; these are composed of 3 to 5, 7 to 12, and 37 to 42 light-dark lamina couplets. Figure 6 illustrates such variations for the case of specimen SC-6. The cycles that are more clearly distinguished are those formed of 7 to 12 light-dark couplets (red lines in Fig. 6). Each of these 7- to 12-couplet cycles begins with a dominance of light laminae at the

lower portion of the cycle, with the light laminae being thicker than the dark laminae. This difference progressively changes upwards, to the point that the thickness of the dark laminae is similar to, or greater than, that of the light laminae at the upper portion of the cycle. Moreover, the dark laminae at the top of these cycles are more continuous laterally than the underlying laminae, and their top boundaries are sharp. Cycles formed of 3 to 5 light-dark lamina couplets (blue lines in Fig. 6) are not so clear. In these 3- to 5-couplet shorter cycles, there is also an upward decrease of the light lamina thickness, at the same time that the dark laminae thicken upward. Moreover, these two order cycles are grouped into higher order cycles that are formed of 38 to 42 light-dark lamina couplets, which are clearly distinguished with the naked eye (black lines in Fig. 6). Lamina accretion patterns similar to those of specimen SC-6 are recognised in specimens PL-22 (Fig. 7) and VS-22 (Supplementary material 2). These two specimens show cycles of 9 to 12 light-dark lamina couplets with the same variations as those found in SC-6.

6.3 Spectral analysis

The spectral analysis reveals several statistically significant power spectrum peaks in Path-A and Path-B. Path-A spectra from specimens PL-22, VS-22, and SC-6 (Fig. 2), show several peaks that are repeated around the same frequency bands in the three specimens (Figs. 8C, 8E, 8F, Supplementary material 3). In contrast, in Path-B spectra from the three same specimens, the statistically significant peaks are distributed in a less defined frequency band, and in general the peaks are less significant than those of Path-A, except at the highest frequencies, where the levels of significance are similar (Figs. 8D, Supplementary material 3). From these considerations, the focus will be on the spectral analysis of Path-A, through flat laminae in the five specimens, and in the cases of domed and columnar internal growth forms, through their flanks.

The results obtained from the spectral analysis performed on the raw luminance data are

essentially similar to those from the lamina thickness data (Supplementary material 4). In most cases the main significant power spectrum peaks are present in the spectra from both types of data. The peaks arise at similar frequencies in thickness and raw luminance based spectra, but the peaks usually have lower confidence levels at lower frequency bands. Spectral analyses from thickness laminae time series reveal more accurate results than raw luminance data time series.

The spectral analysis of light-dark lamina couplets revealed several recurrent periods of thickness variation in the stromatolitic lamination (Figs. 8C, 8E to 8H). The PL-22 spectral analysis (Fig. 8E) detected periodicities around 2.3 years, and at 4.5 and 26.2 years, with a confidence level above 95%. Several peaks in the power spectrum were detected at 3.1, 3.8 and 5 years at a confidence level of over 90%. The VS-22 spectral analysis (Fig. 8F) reveals several statistically significant periods, around 2.5 years, and at 2.8, 3.5, and 22.1 years, exceeding the 95% confidence level. Several significant peaks can be recognised in the AC-5 spectrum (Fig. 8G). The outstanding peaks in the power spectrum, at over 99% confidence level, are at 5.2 and 5.9 years; other periodicities are recognised around 2.5 and 3.7 years, and at 7.7 and 10.2 years, at a confidence level of over 95%. The SC-6 spectral analysis (Fig. 8C) reveals cycles with periods of 2 and 3.7 years, at a confidence level of over 95%. A cycle with a period of 10.6 years arises at over 90%, and very close to the 95% confidence level. As for SC-141 (Fig. 8H), the spectral analysis yields periodicities around 3.6 and 23.6 years, and at 4.7 years, at a confidence level of over 99%; and periodicities around 2.2, 3, and 7.8 years are only observed over 95%. A 10.7 year periodic cycle rises over the 90% confidence level.

Separated spectra can be obtained from light or dark laminae time series (Figs. 8A, 8B, Supplementary material 5). Analyses performed on the thicknesses of light-dark laminae reveal very similar spectral results to those of the light laminae. In contrast, in specimen PL-22, the spectrum resulting from using only the thicknesses of the dark laminae reveals strengthened

peaks reaching higher levels of confidence at 2.2-2.3, 6.4, and 9.9 year cycles (Figs. 8I, Supplementary material 5). In VS-22, the dark laminae spectral analysis shows new significant periods, not detected previously, around 5.5, 6, and 10.5 years, exceeding the 95% confidence level (Figs. 8J, Supplementary material 5). The spectral analysis of the SC-6 dark laminae also reveals other significant cycles, with periods of 2.5, 3.3, 6.5, 8.2, and 10.2 years (Fig. 8B). However, the AC-5 dark laminae thickness spectrum (Figs. 8K, Supplementary material 5) shows similar peaks to those in the light-dark thickness spectrum, except for one peak that marks a period of 21 years with greater significance (above the 90% confidence level). The SC-141 spectrum reveals similar significant periods in the light plus dark, light or dark laminae analyses (Figs. 8L, Supplementary material 5).

The specimens that reveal greater deviations between the spectral analyses of light-dark and light laminae versus dark laminae show higher convexity of the laminae (PL-22, VS-22, and SC-6), while the specimens with flat laminae reveal more similar results among their spectra (AC-5 and SC-141)(Fig. 2).

In specimens that show more convex laminae (PL-22, VS-22, and SC-6), the spectra produced with only the dark lamina thicknesses reveal new power spectrum peaks at frequencies corresponding to intervals with periods between 5 and 22 years (Figs. 8I, 8J, Supplementary material 5). If these frequency peaks were already present in the spectra obtained from the light-dark couplet thicknesses, the periodicities would present a higher significance. A less significant peak is present in the spectral band of periods between 3 and 5 years.

In summary, the Fourier transform spectral analysis of the time series based on the thickness values of light-dark lamina couplets indicates the existence of several significant peaks in the power spectrum density curve (Fig. 8). The power spectrum from the couplet-based time series reveals persistent significant peaks at the 2.2–2.5-year period; the most significant peaks are around the 3.7-year period. Other significant peaks are around the 5- and 6.5-year periods.

In some cases, significant peaks can be recognised around the 8-, 10-, and 20- to 23-year periods. Several peaks exceed the 99% confidence level (e.g., around 2.5, 3.7, 5, 6, and 8). In other cases, the peaks, including those around 10, only reach the 90-95% or 95-99% confidence band. At lower frequencies the peaks are below the 90% confidence band, or have such low frequencies that they are not credible for the time series duration.

The continuous wavelet analysis (Fig. 9) confirms the presence of periodic cycles similar to those found by the singular spectral analysis. The persistence of areas delimited by the 95% confidence level (using the red noise model) through the time represented by the number of lamina couplets indicates the loci where the periodicity is more evident.

7. Discussion

7.1 Annual nature of the lamina couplets

Deciphering the environmental and temporal significance of stromatolite lamination is not easy, due to the wide variety of processes involved (Petryshyn et al., 2012; Arenas and Jones, 2017). In continental contexts, variations in temperature, precipitation and evaporation may directly or indirectly cause the formation of laminae, which in many cases result in texture and colour alternations (Andrews and Brasier, 2005; Kano et al., 2007; Brasier et al., 2010; Frantz et al., 2014; Dabkowski et al., 2015; Bouton et al., 2016), and repetitive lamination (Monty, 1967; Suarez-Gonzalez et al., 2014).

The formation of stromatolite laminae in some spring-tufa and marine deposits has been considered daily (e.g.,Takashima and Kano, 2008; Okumura et al., 2013a, 2013b), seasonal or annual (Hofmann, 1973; Kano et al., 2007; Gradziński, 2010), based on the textural and geochemical characteristics. Based on radiometric ages through stromatolite sections, a multiannual duration has been estimated for some laminae in the Holocene stromatolites of

Walker Lake (Petryshyn et al., 2012). For example, daily cycles have been recognised in the lamination of current travertines due to the activities of microorganisms that favour or inhibit the micrite precipitation (Okumura et al., 2013a). In the fluvial environment, studies of modern stromatolites have shown that several laminae can form in a few months, with periodic and non-periodic climatic parameters influencing the lamina formation (Gradziński, 2010; Arenas and Jones, 2017).

In the lacustrine stromatolites studied herein, the correlation between the stromatolite textural changes and the stable isotopic variations ($\delta^{13}C$ and $\delta^{18}O$) of laminae at different orders relates the light-dark lamina couplet with the seasonal variations in the year (Martin-Bello et al., 2019a). Other time frameworks can be proposed for these couplets. However, if each light-dark lamina of the stromatolites in the Sierra de Alcubierre had formed in a daily cycle, the studied stromatolite specimens would have developed only in a few months. Given that there is no evidence of major interruptions within the studied stromatolite lamination, daily growth is not a reasonable duration for each lamina pair. Longer cycles, such as the Heinrich and Milankovitch cycles, vary on millennial and much longer scale periods. These cycles cannot be reflected in the studied stromatolite specimens of the Sierra de Alcubierre, because the time estimated for the stratigraphic portions, in which the specimens are included, is too short (see Pérez-Rivarés et al., 2018 and reference therein). Therefore, the more coherent duration of each single light-dark lamina couplet of the studied Miocene stromatolites in the Sierra de Alcubierre should be annual, as suggested by Martin-Bello et al. (2019a).

7.2 How fast do stromatolites grow?

Stromatolites are complex three-dimensional structures where the growth rates can vary depending on the stromatolite portion in which they are calculated (Petryshyn et al., 2012). Thus, the growth rates in this work should be considered as an estimation of the order of

magnitude. These results can be compared with rates obtained from stromatolites in other environments and/or from other lacustrine deposits. The mean calculated growth rate of the studied stromatolites is 0.362 mm yr^{-1} (between 0.199 and 0.540 mm yr^{-1}; Table 1). Holocene lacustrine stromatolites from Walker Lake (Nevada) yielded growth rate estimates between 0.066 and 0.390 mm yr^{-1} (Petryshyn et al., 2012). These rates are much lower than those measured in modern riverine stromatolites. For example, in some streams in the Iberian Range, mean rates vary from 4.56 to 13.75 mm yr^{-1} (Arenas et al., 2014, 2015). In recent fluvial laminated tufa of southern Japan, Kano et al. (2007) estimate rates from 2.8 to 11.2 mm $year^{-1}$. These differences are consistent with the idea that lacustrine stromatolites have lower growth rates than fluvial ones, mainly because of the strong and dominant mechanical CO_2-outgassing in most riverine carbonate systems. However, the calculated rate in the Ebro Basin stromatolites is much higher than the average sedimentation rates of the stratigraphic portions in which the stromatolites occur (Fig. 1C). For example, the rate is approximately 0.070 mm yr^{-1} in the dominantly lacustrine portions of unit T6 (Pérez Rivarés, 2016). These circumstances have to be taken into account when calculating average sedimentation rates in stratigraphic intervals containing stromatolitic deposits, as the total rates could otherwise be overestimated.

7.3 Recognition of solar, ENSO, and NAO cycles in the stromatolite lamination

A correlation between the periodic cycles registered in the lamination of the Miocene stromatolites of the Sierra de Alcubierre and the circulation phenomena ENSO and NAO, as well as the solar cycles, can be established from results of three different proxies: luminance and thickness spectral analysis, visual recognition of colour and thickness patterns, and High Resolution Sampling stable isotopic analysis.

Power spectrum and wavelet transform analyses of lamina couplet thickness and luminance time series reveal coherent main modes around 2.5, 3.7, 5, 7, 10, and 22-year periods (Figs. 8,

9; and Supplementary material 3, 4, 5). If each lamina couplet is assumed to represent a year, as reasoned above, the peaks that represent 2.0–2.5 couplets may correspond to the Quasi-Biennial Oscillation (QBO, Baldwin et al., 2001) or the biennial component of ENSO (Rasmusson et al., 1990). The 3–5-couplet peaks may then be indicative of ENSO (Quinn and Neal, 1987; Philander, 1990; Weedon, 2003), and the 5–7-couplet peaks may be linked to the most typical NAO modes (Hurrell and van Loon, 1997). The period at 13 couplets may be linked to low-frequency modes of the NAO (Rossi et al., 2011; Ólafsdóttir et al., 2013); other NAO periods exist, but are not as significant and persistent as the lowest frequency periods.

The Schwabe solar cycle has a period of about 11 years, but varies in duration with a standard deviation of approximately 14 months (Hathaway, 2015). The periods found at 8–11 and 22–23 couplets match the 11-year Schwabe and 22-year Hale sunspot cycles. The persistent period at 26, present in the PL-22 spectrum, might be linked to the AMO variability of 26–28 years (Knudsen et al., 2011; Olsen et al., 2012).

The continuous wavelet transform analyses reveal an intermittent behaviour in the periodicity of the studied time series (quasi-periodic behaviour) that is typical of the NAO/ENSO, with active phases and their corresponding maximum amplitudes in different frequency bands (Brönnimann et al., 2007). The spectrum (Fig. 9) reveals periods of around 2.5 and 6–10 couplets, similar to the classic periods found by Hurrell and van Loon (1997) for the NAO. The peaks of lower frequency should be questioned because the time series have insufficient data to obtain a good estimation in these frequency bands. Although the actual climate indices of different atmospheric phenomena have periods in common (Rossi et al., 2011), the periods obtained from this work have been correlated with the more typical oscillation bands of each phenomenon.

The statistically significant peaks obtained in the power spectrum reveal that correlative patterns defined by the lamina thickness variations can be identified, not only in the spectral

analysis, but also through manual counting on the polished sections. In specimens AC-5 and SC-141, the thickness and colour variation patterns observed on the polished sections (Fig. 2), are not as evident as in specimens PL-22, VS-22, and SC-6 (Figs. 6, 7), because there are wide intervals with similar thicknesses of the laminae, which make it difficult to recognise cycles. The cycles composed of 7 to 12 light-dark couplets (red lines in Fig. 6), which are consistent with the peaks revealed by the spectral analysis of this period band (Fig. 8A to 8D), could correspond to the effects of the NAO and ENSO over the modes of 8 and 11 years, or to the 11-year Schwabe solar cycles. Higher frequency cycles, of 3 to 5 light-dark lamina couplets, are also recognised (blue lines in Fig. 6), but these are not so clear. In this case the pattern could be related to the higher frequency of the NAO and ENSO phenomena. At the same time, higher-order cycles (black lines in Fig. 6) are formed of approximately 40 light-dark lamina couplets, but these are not reflected in the spectral analysis due to the limited number of laminae that compose the specimen. Some atmospheric circulation phenomena have modal variations around these values, such as the AMO, with a period of 40 years. Specimens PL-22 (Fig. 7) and VS-22 (Supplementary material 2) show cycles of 9 to 12 light-dark lamina couplets (red lines) as in SC-6. These couplets could be related to the peaks obtained through the spectral analysis of this specimen, better marked by the dark lamina thicknesses (Fig. 8I, 8J), and ultimately to the 11-year Schwabe solar cycles. In turn, the 3 to 6 light-dark lamina couplets (blue lines in Figs. 7, Supplementary material 2) can also be related to the higher-frequency modes of the NAO and ENSO phenomena. In specimens PL-22 and VS-22, higher rank cycles formed of 26 and 22 light-dark lamina couplets (black lines in Figs. 7, Supplementary material 2), respectively, are also revealed by the spectral analysis. These cycles could be linked to the 22-year Hale solar cycle.

Results from high-resolution isotopic analyses performed in specimen PL-22 (Fig. 7) by Martin-Bello et al. (2019a) support that the third order isotopic cycles (Figs. 5A, 4A, 4B), represented by light-dark lamina couplets, correspond to annual lamination. Likewise, the results of the

spectral analyses reveal that the second order isotopic cycles can be correlated with the cycles of lamina couplets with periods around 3.5, 5, 6, and 8 years, which are related to the NAO/ENSO circulation phenomena. The first order isotopic cycles, which are the lowest frequency cycles, can be identified with the cycles consisting of 9–12 couplets that are related to lower frequency modes of the NAO/ENSO, or directly with the 11-year solar cycles.

The varying quality of the spectra results obtained in this study is consistent with present-day observations of the NAO and, at the same time, fits the interpretation of lamina formation proposed by Martin-Bello et al. (2019a). The anti-cyclonic activity that occurs during the positive phase of the NAO has been associated with a greater possibility of drought in the eastern part of the Iberian Peninsula (Pozo-Vázquez et al., 2001; Muñoz-Díaz and Rodrigo, 2004, 2006). However, the influence of the NAO on the probability of abundant rainfall, and therefore of rainy winters in this area, is less evident. This could explain why better results are obtained in the 5- to 8- year period band (related to circulation phenomena of the NAO/ENSO) of the spectra based on time series of dark laminae (formed in drier conditions in the summer) than in those based on light laminae and dark-light lamina couplets.

The longer cycles reflected in the Miocene stromatolites of this study (i.e., 8–23 years) can be attributed to the 11-year Schwabe and 22-year Hale solar cycles. However, these cycles could also have been produced by the higher typical modes of the NAO and ENSO. There is evidence, based on observation and simulation processes, of a direct relation between solar cycles and atmospheric circulation patterns like the NAO (Kodera and Kuroda, 2005; Gray et al., 2016; Li and Xiao, 2018) and ENSO (Nuzhdina, 2002; Zhai, 2017). We do not reject the possibility that the solar cycles could have indirectly influenced the lamina accretion of the stromatolites through variations in humidity influenced by the NAO and ENSO, rather than only directly through solar irradiance. This indirect solar influence is suggested by the irregular occurrence of the 8- to 23-year cycles in the spectra and the wavelets of the several specimens studied

here. This result is in accordance with the periods of around 10 and 21 years that are obtained from the El Niño No. 3 area index (Cook, 2000), which has been related to solar activity (Hathaway, 2015; Zhai, 2017). The close relationship between the quasi-periodic variations of these phenomena makes it difficult to discriminate the different contributions of each of them in a particular time interval of the studied stromatolite growth. As it happens nowadays, both circulation patterns (NAO and ENSO) could also coexist in the Oligocene or Miocene (Walliser et al., 2017). The results from the stromatolite periodic analysis in the Ebro Basin fit such a hypothesis and suggest influences of the three phenomena (solar activity, either directly or indirectly, and the precursors of NAO and ENSO) on the middle Miocene climate of the north-eastern Iberian Peninsula.

8. Conclusions

This study provides convincing evidence of the utility of spectral analysis (Fourier transform and wavelet spectral analyses) for understanding climatic influence on stromatolite lamination at several time scales. A periodicity analysis was performed on several Miocene lacustrine stromatolites in the Ebro Basin, Spain. Assuming that each light-dark lamina couplet represents a year, as supported by textural and stable isotope analyses by Martin-Bello et al. (2019a), the periodic cycles found in this study can be related to some of the main variability modes of atmospheric circulation phenomena like the NAO and ENSO, and solar activity. The periodicity analysis was performed over several time series, based on lamina thicknesses and luminance measurements through different paths in several stromatolites. The results reveal consistent periods, and exceed very high confidence levels. From these results the following important conclusions can be drawn:

1. From a methodological point of view, in this study, the results of time-series spectral analysis based on lamina thickness data were more accurate than those from the analysis

based on raw luminance data. The time-series obtained through flat-lamina sections yielded more significant results than those obtained through convex-lamina sections of the specimens. Indeed, some frequency bands were only significant in time-series based solely on one type of lamina (i.e., the dark lamina).

2. The fact that analysis of dark lamina produces more significant results than light or light-dark laminae in some frequency bands (5 to 22) might suggest that sedimentary records formed in the dry and/or warm seasons are better records of climate variations at decadal or multi-decadal scales.

3. The annual duration assumed for each light-dark lamina couplet implies that the lifespan of the studied stromatolite specimens is between 120 and 500 years. The growth rates of these stromatolites vary between 0.199 and 0.540 mm yr^{-1}.

4. Time-series analysis shows persistent significant periods over 2.5, 3.7, 5, 7, 10, and 22 years. Even though this distribution of periods is common to several climate phenomena and solar activity, these periods can be associated with the typical oscillation bands of specific climatic signatures. The 2.5-year periods correspond to the QBO or the biennial component of the ENSO or NAO variability. Periods within 3 to 5 and 5 to 7-year bands can be linked to typical NAO or ENSO variability. The periods of 8 to 11 and 22 to 23-year bands match the 11-year Schwabe and 22-year Hale sunspot cycles. Thus, in this study, there is not a simple solution about the contribution of each of these phenomena to lamina periodicity.

5. There is a correlation between the cyclicity orders based on stable isotope analyses from Martin-Bello et al. (2019a) and the periods and climatic signatures presented in this study. Third-order cycles are identified with the light-dark simple lamina couplets (annual cycles) used in the spectral analysis. Second-order cycles (each dark and each light composite laminae) can be correlated with the cycles of lamina couplets with periods around 3.5, 5, 6, and 8 years, which are related to NAO/ENSO variability. First order cycles (each pair of consecutive light and dark composite laminae) are identified with 9–12 couplets, and are

related to NAO/ENSO-like or 11-years Schwabe solar cycles.

6. The persistent significant periods detected by the time series analysis in the studied Miocene stromatolites reveal inter-annual, decadal, and even multi-decadal climatic variability, which reinforces the evidence of the presence of ENSO and NAO precursors during the Miocene.

Aknowledgements

This work was supported by the project CGL2013-42867-P and FPI contract BES-2014-069389 of the Spanish Government and European Regional Funds. F.J. Pérez-Rivarés held a contract from the project CGL2013-42867-P. The results are also part of the activities of the Geotransfer scientific group (Aragón Government, Operating Program FEDER Aragón 2014-2020). We are grateful to Dr. C. Osácar and Dr. L. Auqué for their help at several steps of this work. Dr G. Pardo is sincerely thanked for his helpful comments and suggestions on the manuscript. Two anonymous reviewers and the Editor-in-Chief C. Chagué helped improve the manuscript.

References

Affek, H.P., 2012. Clumped isotope paleothermometry: principles, applications, and challenges. The Paleontological Society Papers 18, 101–114.

Andrews, J.E., Brasier, A.T., 2005. Seasonal records of climatic change in annually laminated tufas: Short review and future prospects. Journal of Quaternary Science 20, 411–421.

Arche, A., Evans, G., Clavell, E., 2010. Some considerations on the initiation of the present SE Ebro river drainage system: Post- or pre-Messinian? Journal of Iberian Geology 36, 73–85.

Arenas, C., Auqué, L., Osácar, C., Sancho, C., Lozano, M.V., Vázquez-Urbez, M., Pardo, G., 2015. Current tufa sedimentation in a high discharge river: A comparison with other synchronous tufa records in the Iberian Range (Spain). Sedimentary Geology 325, 132–157.

Arenas, C., Casanova, J., Pardo, G., 1997. Stable isotope characterization of the Miocene lacustrine systems of Los Monegros (Ebro Basin, Spain): palaeogeographic and palaeoclimatic implications. Palaeogeography, Palaeoclimatology, Palaeoecology 128, 133–155.

Arenas, C., Jones, B., 2017. Temporal and environmental significance of microbial lamination: Insights from Recent fluvial stromatolites in the River Piedra, Spain. Sedimentology 64, 1597–1629.

Arenas, C., Pardo, G., 1999. Latest Oligocene-Late Miocene lacustrine systems of the north-central part of the Ebro Basin (Spain): Sedimentary facies model and palaeogeographic synthesis. Palaeogeography, Palaeoclimatology, Palaeoecology 151, 127–148.

Arenas, C., Osácar, M.C., Auqué, L., Sancho, C., 2019. Coupling textural and stable-isotope variations in fluvial stromatolites: Comparison of Pleistocene and recent records in NE Spain. Journal of Paleogeography 8, 13. https://doi.org/10.1186/s42501-019-0021-y

Arenas, C., Vázquez-Urbez, M., Auqué, L., Sancho, C., Osácar, C., Pardo, G., 2014. Intrinsic and extrinsic controls of spatial and temporal variations in modern fluvial tufa sedimentation: A thirteen-year record from a semi-arid environment. Sedimentology 61, 90–132.

Arp, G., Bielert, F., Hoffmann, V.E., Löffler, T., 2005. Palaeoenvironmental significance of lacustrine stromatolites of the Arnstadt Formation (“Steinmergelkeuper”, Upper Triassic,

N-Germany). Facies 51, 419–441.

Arp, G., Bissett, A., Brinkmann, N., Cousin, S., De Beer, D., Friedl, T., Mohr, K.I., Neu, T.R., Reimer, A., Shiraishi, F., Stackebrandt, E., Zippel, B., 2010. Tufa-forming biofilms of German karstwater streams: microorganisms, exopolymers, hydrochemistry and calcification. Journal of the Geological Society of London Special Publication 336, 83–118.

Baldwin, M.P., Gray, L.J., Dunkerton, T.J., Hamilton, K., Haynes, P.H., Holton, J.R., Alexander, M.J., Hirota, I., Horinouchi, T., Jones, D.B.A., Marquardt, C., Sato, K., Takahashi, M., 2001. The Quasi-Biennial Oscillation. Reviews of Geophysics 39, 179–229.

Batenburg, S.J., Reichart, G.J., Jilbert, T., Janse, M., Wesselingh, F.P., Renema, W., 2011. Interannual climate variability in the Miocene: High resolution trace element and stable isotope ratios in giant clams. Palaeogeography, Palaeoclimatology, Palaeoecology 306, 75–81.

Beer, J., Mende, W., Stellmacher, R., 2000. The role of the sun in climate forcing. Quaternary Science Reviews 19, 403–415.

Bice, K.L., Scotese, C.R., Seidov, D., Barron, E.J., 2000. Quantifying the role of geographic change in Cenozoic ocean heat transport using uncoupled atmosphere and ocean models. Palaeogeography, Palaeoclimatology, Palaeoecology 161, 295–310.

Bond, G., Showers, W., Cheseby, M., Lotti, R., Almasi, P., Demenocal, P., Priore, P., Cullen, H., Hajdas, I., Bonani, G., 1997. A pervasive millennial-scale cycle in North Atlantic Holocene and glacial climates. Science 278, 1257–1266.

Bouton, A., Vennin, E., Pace, A., Bourillot, R., Dupraz, C., Thomazo, C., Brayard, A., Desaubliaux, G., Visscher, P.T., 2016. External controls on the distribution, fabrics and mineralization

of modern microbial mats in a coastal hypersaline lagoon, Cayo Coco (Cuba). Sedimentology 63, 972–1016.

Brachert, T.C., Reuter, M., Felis, T., Kroeger, K.F., Lohmann, G., Micheels, A., Fassoulas, C., 2006. Porites corals from Crete (Greece) open a window into Late Miocene (10 Ma) seasonal and interannual climate variability. Earth and Planetary Science Letters 245, 81–94.

Brasier, A.T., Andrews, J.E., Marca-Bell, A.D., Dennis, P.F., 2010. Depositional continuity of seasonally laminated tufas: Implications for $\delta^{18}O$ based palaeotemperatures. Global and Planetary Change 71, 160–167.

Brönnimann, S., Xoplaki, E., Casty, C., Pauling, A., Luterbacher, J., 2007. ENSO influence on Europe during the last centuries. Climate Dynamics 28, 181–197.

Catalan, J., Pla-Rabés, S., Wolfe, A.P., Smol, J.P., Rühland, K.M., Anderson, N.J., Kopácek, J., Stuchlík, E., Schmidt, R., Koinig, K.A., Camarero, L., Flowe,r R.J., Heiri, O., Kamenik, C., Korhola, A., Leavitt, P.R., Psenner, R., Renberg, I., 2013. Global change revealed by palaeolimnological records from remote lakes: a review. Journal of Paleolimnology 49, 513– 535.

Cook, E.R., 2000. Niño 3 Index Reconstruction. International Tree-Ring Data Bank. IGBP PAGES/World Data Center-A for Paleoclimatology. Data Contribution Series #2000-052.NOAA/NGDC Paleoclimatology Program, Boulder, CO, USA.

Costa, E., Garcés, M., López-Blanco, M., Beamud, E., Gómez-Paccard, M., Larrasoaña, J.C., 2010. Closing and continentalization of the South Pyrenean foreland basin (NE): magnetochronological constraints. Basin Research 22, 904–917.

Dabkowski, J., Royle, S.H., Antoine, P., Marca-Bell, A., Andrews, J.E., 2015. High-resolution $\delta^{18}O$

seasonality record in a French Eemian tufa stromatolite (Caours, Somme Basin). Palaeogeography, Palaeoclimatology, Palaeoecology 438, 277–284.

Dasarathy, B.V. (Ed.), 1991. Nearest Neighbor: Pattern Classification Techniques IEEE. Computer Society Press, Los Alamitos.

Fraedrich, K., Muller, K., 1992. Climate anomalies in Europe associated with ENSO extremes. International Journal of Climatology 12, 25–31.

Frantz, C.M., Petryshyn, V.A., Marenco, P.J., Tripati, A., Berelson, W.M., Corsetti, F.A., 2014. Dramatic local environmental change during the Early Eocene Climatic Optimum detected using high resolution chemical analyses of Green River Formation stromatolites. Palaeogeography, Palaeoclimatology, Palaeoecology 405, 1–15.

Galeotti, S., von der Heydt, A., Huber, M., Bice, D., Dijkstra, H., Jilbert, T., Lanci, L., Reichart, G.J., 2010. Evidence for active El Niño Southern Oscillation variability in the Late Miocene greenhouse climate. Geology 38, 419–422.

Goodess, C.M., Jones, P.D., 2002. Links between circulation and changes in the characteristics of Iberian rainfall. International Journal of Climatology 22, 1593–1615.

Gradziński, M., 2010. Factors controlling growth of modern tufa: results of a field experiment. Journal of the Geological Society of London Special Publication 336, 143–191.

Gray, L.J., Beer, J., Geller, M., Haigh, J.D., Lockwood, M., Matthes, K., Cubasch, U., Fleitmann, D., Harrison, G., Hood, L., Luterbacher, J., Meehl, G.A., Shindell, D., Van Geel, B., White, W., 2010. Solar influences on climate. Reviews of Geophysics 48, RG4001. https://doi.org/10.1029/2009RG000282

Gray, L.J., Woollings, T.J., Andrews, M., Knight, J., 2016. Eleven-year solar cycle signal in the

NAO and Atlantic/European blocking. Quarterly Journal of the Royal Meteorological Society 142, 1890–1903.

Hammer, Ø., Harper, D.A.T., Ryan, P.D., 2001. PAST: Paleontological Statistics Soft-ware Package for Education and Data Analysis. Palaeontologia Electronica 4, 1–9. https://doi.org/http://palaeo-electronica.org/2001 1/past/issue1 01.htm

Hathaway, D.H., 2015. The solar cycle. Living Reviews in Solar Physics 12, 4. https://doi.org/10.1007/lrsp-2015-4

Hernández-Ballarín, V., Peláez-Campomanes, P., 2017. Impact of global climate in the diversity patterns of middle Miocene rodents from the Madrid Basin (Spain). Palaeogeography, Palaeoclimatology, Palaeoecology 472, 108–118.

Hofmann, H.J., 1973. Stromatolites: Characteristics and Utility. Earth-Sciences Reviews 9, 339–373.

Holbourn, A.E., Kuhnt, W., Clemens, S.C., Kochhann, K.G.D., Jöhnck, J., Lübbers, J., Andersen, N., 2018. Late Miocene climate cooling and intensification of southeast Asian winter monsoon. Nature Communications 9, 1584. https://doi.org/10.1038/s41467-018-03950-1

Holmgren, K., Karlén, W., Lauritzen, S.E., Lee-Thorp, J.A., Partridge, T.C., Piketh, S., Repinski, P., Stevenson, C., Svanered, O., Tyson, P.D., 1999. A 3000-year high-resolution stalagmite-based record of palaeoclimate for northeastern South Africa. The Holocene 9, 295–309.

Huber, M., Caballero, R., 2003. Eocene El Niño: Evidence for robust tropical dynamics in the "Hothouse." Science 299, 877–881.

Hurrell, J. W., 1995. Decadal trends in the North Atlantic oscillation: Regional temperatures and precipitation. Science 269, 676–679.

Hurrell, J.W., Kushnir, Y., Ottersen, G., Visbeck, M., 2003. An overview of the North Atlantic Oscillation. Geophysical Monograph 134, 1–35.

Hurrell, J. W., van Loon, H., 1997. Decadal variations in climate associated with the North Atlantic Oscillation. Climatic Change 36, 301–326.

Hwang, C., Peng, M.F., Ning, J., Luo, J., Sui, C.H., 2005. Lake level variations in China from TOPEX/Poseidon altimetry: data quality assessment and links to precipitation and ENSO. Geophysical Journal International 161, 1–11.

Jones P.D., Osborn T.J., Briffa K.R., 2003. Pressure-based measures of the North Atlantic Oscillation (NAO): a comparison and an assessment of changes in the strength of the NAO and its influence on surface climate parameters. In: Hurrell, J.W., Kushnir, Y., Ottersen, G., Visbeck, M., (Eds.), The North Atlantic Oscillation: climatic significance and environmental impact. American Geophysical Union, Washington, DC, pp. 51–62

Kalimeris, A., Ranieri, E., Founda, D., Norrant, C., 2017. Variability modes of precipitation along a Central Mediterranean area and their relations with ENSO, NAO, and other climatic patterns. Atmospheric Research 198, 56–80.

Kano, A., Hagiwara, R., Kawai, T., Hori, M., Matsuoka, J., 2007. Climatic conditions and hydrological change recorded in a high-resolution stable-isotope profile of a recent laminated tufa on a subtropical island, southern Japan. Journal of Sedimentary Research 77, 59–67.

Kano, A., Matsuoka, J., Kojo, T., Fujii, H., 2003. Origin of annual laminations in tufa deposits, southwest Japan. Palaeogeogrraphy, Palaeoclimatology, Palaeoecology 191, 243–262.

Kato, H., Amekawa, S., Kano, A., Mori, T., Kuwahara, Y., Quade, J., 2019. Seasonal temperature changes obtained from carbonate clumped isotopes of annually laminated tufas from Japan: Discrepancy between natural and synthetic calcites. Geochimica et Cosmochimica Acta 244, 548–564.

Kele, S., Breitenbach, S.F.M., Capezzuoli, E., Meckler, A.N., Ziegler, M., Millan, I.M., Kluge, T., Deák, J., Hanselmann, K., John, C.M., Yan, H., Liu, Z., Bernasconi, S.M., 2015. Temperature dependence of oxygen- and clumped isotope fractionation in carbonates: A study of travertines and tufas in the 6-95°C temperature range. Geochimica et Cosmochimica Acta 168, 172–192.

Kelts, K., Talbot, M., 1990. Lacustrine carbonates as geochemical archives of environmental change and biotic/abiotic interactions. In: Tilzer, M.M., Serruya, C. (Eds.), Large Lakes: Ecological Structure and Function. Springer-Verlag, Berlin, pp. 288–315.

Kennard, J.M., Burne, R.V., 1989. Stromatolite Newsletter Number 14. Bureau of Mineral Resources, Geology and Geophysics, Camberra.

Kloosterboer-Van Hoeve, M.L., Steenbrink, J., Visscher, H., Brinkhuis, H., 2006. Millennial-scale climatic cycles in the Early Pliocene pollen record of Ptolemais, northern Greece. Palaeogeography, Palaeoclimatology, Palaeoecology 229, 321–334.

Knippertz, P., Ulbrich, U., Marques, F., Corte-Real, J., 2003. Decadal changes in the link between El Niño and springtime North Atlantic Oscillation and European–North African rainfall. International Journal of Climatology 23, 1293–1311

Knudsen, M.F., Seidenkrantz, M-S., Jacobsen, B.H., Kuijpers, A., 2011. Tracking the Atlantic Multidecadal Oscillation through the last 8,000 years. Nature Communications 2, 178. https://doi.org/10.1038/ncomms1186

Kodera, K., Kuroda, Y., 2005. A possible mechanism of solar modulation of the spatial structure of the North Atlantic Oscillation. Journal of Geophysical Research 110, D02111. https://doi.org/10.1029/2004JD005258

Laskar, J., Robutel, P., Joutel, F., Gastineau, M., Correia, A.C.M., Levrard, B., 2004. A long-term numerical solution for the insolation quantities of the Earth. Astronomy & Astrophysics 428, 261–285.

Lau, K.-M., Weng, H., 1995. Climate signal detection using wavelet transform: How to make a time series sing. Bulletin of the American Meteorological Society 76, 2391–2402.

Leng, M.J., Marshall, J.D., 2004. Palaeoclimate interpretation of stable isotope data from lake sediment archives. Quaternary Science Reviews 23, 811–831.

Lenz, O.K., Wilde, V., Riegel, W., Harms, F.J., 2010. A 600 k.y. record of El Niño-Southern Oscillation (ENSO): Evidence for persisting teleconnections during the Middle Eocene greenhouse climate of Central Europe. Geology 38, 627–630.

Li, D., Xiao, Z., 2018. Can solar cycle modulate the ENSO effect on the Pacific/North American pattern? Journal of Atmospheric and Solar-Terrestrial Physics 167, 30–38.

López-Blanco, C., Andrews, J., Dennis, P., Rosa, M., Vicente, E., 2016. North Atlantic Oscillation recorded in carbonate δ18O signature from Lagunillo del Tejo (Spain). Palaeogeography, Palaeoclimatology, Palaeoecology 441, 882–889.

Manzo, E., Perri, E., Tucker, M.E., 2012. Carbonate deposition in a fluvial tufa system: Processes and products (Corvino Valley - southern Italy). Sedimentology 59, 553–577.

Margalef, R., 1983. Limnología. Editorial Omega, Barcelona. (in Spanish)

Martin-Bello, L., Arenas, C., Andrews, J., Alonso-Zarza, A.M., Marca, A., 2019a. Multi-scale records of climate change in lacustrine stromatolites: insights from the Miocene Ebro Basin. Palaeogeography, Palaeoclimatology, Palaeoecology 530, 312–329.

Martin-Bello, L., Arenas, C., Jones, B., 2019b. Lacustrine stromatolites: Useful structures for environmental interpretation - an example from the Miocene Ebro Basin. Sedimentology 66. https://doi.org/10.1111/sed.12577

Matsuoka, J., Kano, A., Oba, T., Watanabe, T., Sakai, S., Seto, K., 2001. Seasonal variation of stable isotopic compositions recorded in a laminated tufa, SW Japan. Earth and Planetary Science Letters 192, 31–44.

Mercier, F., Cazenave, A., Maheu, C., 2002. Interannual lake level fluctuations (1993–1999) in Africa from Topex/Poseidon: connections with ocean-atmosphere interactions over the Indian Ocean. Global and Planetary Change 32, 141–163.

Mertz-Kraus, R., Brachert, T.C., Reuter, M., Galer, S.J.G., Fassoulas, C., Iliopoulos, G., 2009. Late Miocene sea surface salinity variability and paleoclimate conditions in the Eastern Mediterranean inferred from coral aragonite $\delta^{18}O$. Chemical Geology 262, 202–216.

Mingram, J., 1998. Laminated Eocene maar-lake sediments from Eckfeld (Eifel region, Germany) and their short-term periodicities. Palaeogeography, Palaeoclimatology, Palaeoecology 140, 289–305.

Mischke, S., Zhang, C., 2008. A laminated tufa carbonate from the mid Holocene of the Qilian Mountains and its potential for palaeoclimate inferences. Episodes 31, 401–407.

Monty, C.L.V., 1967. The origin and development of cryptalgal fabrics. In: Walter, M.R., (Ed.), Stromatolites. Elsevier, Amsterdam, pp. 193–249.

Muñoz, A., Arenas, C., González, A., Luzón, A., Pardo, G., Pérez, A., Villena, J., 2002a. Ebro basin (northeastern Spain). In: Gibbons, W., Moreno, T. (Eds.), The Geology of Spain.The Geological Society, Londres, pp. 301–309.

Muñoz, A., Bartolomé, M., Muñoz, A., Sancho, C., Moreno, A., Hellstrom, J.C., Osácar, M.C., Cacho, I., 2015. Solar influence and hydrological variability during the Holocene from a speleothem annual record (Molinos Cave, NE Spain). Terra Nova 27, 300–311.

Muñoz, A., Ojeda, J., Sánchez-Valverde, B., 2002b. Sunspot-like and ENSO/NAO-like periodicities in lacustrine laminated sediments of the Pliocene Villarroya Basin (La Rioja, Spain). Journal of Paleolimnology 27, 453–463.

Muñoz-Díaz, D., Rodrigo, F.S., 2004. Impacts of the North Atlantic Oscillation on the probability of dry and wet winters in Spain. Climate Research 27, 33–43.

Muñoz-Díaz, D., Rodrigo, F.S., 2006. Seasonal rainfall variations in Spain (1912-2000) and their links to atmospheric circulation. Atmospheric Research 81, 94–110.

Ndiaye, M., Davaud, E., Ariztegui, D., Fall, M., 2012. A semi automated method for laminated sediments analysis. International Journal of Geosciences 3, 206–210.

Nehza, O., Woo, K.S., Lee, K.C., 2009. Combined textural and stable isotopic data as proxies for the mid-Cretaceous paleoclimate: A case study of lacustrine stromatolites in the Gyeongsang Basin, SE Korea. Sedimentary Geology 214, 85–99.

Nuzhdina, M.A., 2002. Connection between ENSO phenomena and solar and geomagnetic activity. Natural Hazards and Earth System Sciences 2, 83–89.

Okonkwo, C., Demoz, B., Gebremariam, S., 2014. Characteristics of Lake Chad level variability and links to ENSO, precipitation, and river discharge. The Scientific World Journal 2014,

145893, https://doi.org/10.1155/2014/145893

Okumura, T., Takashima, C., Kano, A., 2013a. Textures and processes of laminated travertines formed by unicellular cyanobacteria in Myoken hot spring, southwestern Japan. Island Arc 22, 410–426.

Okumura, T., Takashima, C., Shiraishi, F., Nishida, S., Kano, A., 2013b. Processes forming daily lamination in a microbe-rich travertine under low flow condition at the Nagano-yu Hot Spring, Southwestern Japan. Geomicrobiology Journal 30, 910–927.

Ólafsdóttir, K.B., Geirsdóttir, Á., Miller, G.H., Larsen, D.J., 2013. Evolution of NAO and AMO strength and cyclicity derived from a 3-ka varve-thickness record from Iceland. Quaternary Science Reviews 69, 142–154.

Olsen, J., Anderson, N.J., Knudsen, M.F., 2012. Variability of the North Atlantic Oscillation over the past 5,200 years. Nature Geoscience 5, 808–812.

Osácar, M.C., Arenas, C., Vazquez-Urbez, M., Sancho, C., Auque, L.F., Pardo, G., 2013. Environmental factors controlling the $\delta^{13}C$ and $\delta^{18}O$ variations of recent fluvial tufas: A 12-year record from the Monasterio de Piedra Natural Park (NE Iberian Peninsula). Journal of Sedimentary Research 83, 309–322.

Pardo, G., Arenas, C., González, A., Luzón, A., Muñoz, A., Pérez, A., Pérez-Rivarés, F.J., Vázquez-Urbez, M., Villena, J., 2004. La Cuenca del Ebro, in: Vera, J.A. (Ed.), Geología de España. SGE-IGME, Madrid, pp. 533–543. (In Spanish)

Pérez Rivarés, F.J., 2016. Estudio magnetoestratigráfico del Mioceno del sector central de la Cuenca del Ebro: Cronología, correlación y análisis de la ciclicidad sedimentaria. PhD Thesis. University of Zaragoza. https://zaguan.unizar.es/record/79504 (In Spanish)

Pérez-Rivarés, F.J., Arenas, C., Pardo, G., Garcés, M., 2018. Temporal aspects of genetic stratigraphic units in continental sedimentary basins: Examples from the Ebro basin, Spain. Earth-Sciences Reviews 178, 136–153.

Pérez-Rivarés, F.J., Garcés, M., Arenas, C., Pardo, G., 2002. Magnetocronología de la sucesión miocena de la Sierra de Alcubierre (sector central de la Cuenca del Ebro). Revista de la Sociedad Geológica España 15, 217–231. (in Spanish with English abstract)

Petryshyn, V.A., Corsetti, F.A., Berelson, W.M., Beaumont, W., Lund, S.P., 2012. Stromatolite lamination frequency, Walker Lake, Nevada: Implications for stromatolites as biosignatures. Geology 40, 499–502.

Petryshyn, V.A., Lim, D., Laval, B.L., Brady, A., Slater, G., Tripati, A.K., 2015. Reconstruction of limnology and microbialite formation conditions from carbonate clumped isotope thermometry. Geobiology 13, 53–67.

Philander, S.G.H. (Ed.), 1990. El Niño, La Niña, and the Southern Oscillation. International Geophysics Series, 46. Academic Press 293 pp.

Pozo-Vázquez, D., Esteban-Parra, M.J., Rodrigo, F.S., Castro-Díez, Y., 2001. A study of NAO variability and its possible non- linear influence on European surface temperature. Climate Dynamics 17, 701–715.

Pozo-Vázquez, D., Esteban-Parra, M.J., Rodrigo, F.S., Castro-Diez, Y., 2000. An analysis of the variability of the North Atlantic Oscillation in the time and the frequency domain. International Journal of Climatology 20, 1675–1692.

Quinn, W.H., Neal, V.T., 1987. El Niño occurrences over the past four and a half centuries. Journal of Geophysical Research 92, 14449–14461.

Rasmusson, E.M., Wang, X., Ropelewski, C.F., 1990. The biennial component of ENSO variability. Journal of Marine Systems 1, 71–96.

Reid, G.C., 2000. Solar variability and the earth's climate: introduction and overview. Space Science Reviews 94, 1–11.

Riba, O., Reguant, S., Villena, J., 1983. Ensayo de síntesis estratigráfica y evolutiva de la cuenca terciaria del Ebro. In: Comba, J.A., (Ed.), Geología de España, Libro Jubilar J.M. Ríos. Instituto Geológico y Minero de España, pp. 131–159. (in Spanish)

Riding, R., 2000. Microbial carbonates: the geological record of calcified bacterial-algal mats and biofilms. Sedimentology 47, 179–214.

Rocha, A., 1999. Low-frequency variability of seasonal rainfall over the Iberian Peninsula and ENSO. International Journal of Climatology 19, 889–901.

Rodó, X., Baert, E., Comín, F.A., 1997. Variations in seasonal rainfall in Southern Europe during the present century: relationships with the North Atlantic Oscillation and the El Niño-Southern Oscillation. Climate Dynamics 13, 275–284.

Rodríguez-Berriguete, Á., Alonso-Zarza, A.M., Martín-García, R., Cabrera, M. del C., 2018. Sedimentology and geochemistry of a human-induced tufa deposit: Implications for palaeoclimatic research. Sedimentology 13, 2253–2277.

Rossi, A., Massei, N., Laignel, B., 2011. A synthesis of the time-scale variability of commonly used climate indices using continuous wavelet transform. Global and Planetary Change 78, 1–13.

Scholz, D., Frisia, S., Borsato, A., Spötl, C., Fohlmeister, J., Mudelsee, M., Miorandi, R., Mangini, A., 2012. Holocene climate variability in north-eastern Italy: Potential influence of the

NAO and solar activity recorded by speleothem data. Climate of the Past 8, 1367–1383.

Schulz, M., Mudelsee, M., 2002. REDFIT: estimating red-noise spectra directly from unevenly spaced paleoclimatic time series. Computers & Geosciences 28, 421–426.

Scotese, C.R., 2014. Atlas of Neogene Paleogeographic Maps (Mollweide Projection), Maps 1-7, PALEOMAP Atlas for ArcGIS, Volume 1, the Cenozoic, PALEOMAP Project, Evanston, IL. https://www.academia.edu/11082185/Atlas_of_Neogene_Paleogeographic_Maps.

Seton, M., Müller, R.D., Zahirovic, S., Gaina, C., Torsvik, T., Shephard, G., Talsma, A., Gurnis, M., Turner, M., Maus, S., Chandler, M., 2012. Global continental and ocean basin reconstructions since 200Ma. Earth-Sciences Reviews 113, 212–270.

Shaman, J., Tziperman, E., 2011. An atmospheric teleconnection linking ENSO and Southwestern European precipitation. Journal of Climate 24, 124–139.

Straile, D., Livingstone, D.M., Weyhenmeyer, G.A., Glen George, D., 2003. The response of freshwater ecosystems to climate variability associated with the North Atlantic Oscillation. American Geophysical Union Monograph Series 134, 263–279.

Suarez-Gonzalez, P., Quijada, I.E., Benito, M.I., Mas, R., Merinero, R., Riding, R., 2014. Origin and significance of lamination in Lower Cretaceous stromatolites and proposal for a quantitative approach. Sedimentary Geology 300, 11–27.

Takashima, C., Kano, A., 2008. Microbial processes forming daily lamination in a stromatolitic travertine. Sedimentary Geology 208, 114–119.

Tang, D., Shi, X., Jiang, G., 2014. Sunspot cycles recorded in Mesoproterozoic carbonate biolaminites. Precambrian Research 248, 1–16.

Thomson, D.J., 1990. Time series analysis of Holocene climate data. Philosophical Transactions

of the Royal Society of London 330, 601-660.

Torrence, C., Compo, G.P., 1998. A practical guide to wavelet analysis. Bulletin of the American Meteorological Society 79, 61–78.

Vázquez-Urbez, M., Arenas, C., Pardo, G., Pérez-Rivarés, J., 2013. The effect of drainage reorganization and climate on the sedimentologic evolution of intermontane lake systems: The final fill stage of the Tertiary Ebro Basin (Spain). Journal of Sedimentary

Vicente-Serrano, S.M., 2005. El Niño and La Niña influence on droughts at different timescales in the Iberian Peninsula. Water Resources Research 41, W12415. https://doi.org/10.1029/2004WR003908

Walliser, E.O., Lohmann, G., Niezgodzki, I., Schöne, B.R., 2017. Inter-annual climate variability in Europe during the Oligocene icehouse. Palaeogeography, Palaeoclimatology, Palaeoecology 475, 140–153.

Weedon, G.P., 1993. The recognition and stratigraphic implications of orbital-forcing of climate and sedimentary cycles. In: Wright, V.P., (Ed.), Sedimentology Review, Blackwell, Oxford, pp. 31-50. http://dx.doi.org/10.1002/9781444304534.ch3

Weedon, G.P., 2003. Time-Series Analysis and Cyclostratigraphy. Cambridge University Press, Cambridge. https://doi.org/10.1017/CBO9780511535482

Zhai, Q., 2017. Evidence for the effect of sunspot activity on the El Niño/Southern Oscillation. New Astronomy 52, 1–7.

Zorita E., Kharin V., Von Storch, H., 1992. The atmospheric circulation and sea surface temperature in the North Atlantic area in winter: their interaction and relevance for Iberian precipitation. Journal of Climate 5, 1097–1108.

Figure captions

Figure 1. A) Location of the Ebro Basin in the northeast of the Iberian Peninsula. B) Distribution of lithofacies and genetic stratigraphic units (T5, T6 and T7) through the Sierra de Alcubierre (Ebro Basin, Spain). The positions of the stratigraphic sections are marked: Valle de Soler (VS), Puig Ladron (PL), San Caprasio (SC) and Aldea del Correo (AC). C) Stratigraphic sections with the locations of the studied stromatolite specimens, and chronostratigraphic and magnetostratigraphic sketches based on Pérez-Rivarés et al. (2018). GPTS: Geomagnetic Polarity Time Scale.

Figure 2. Polished sections of the studied stromatolite specimens. VS-22, PL-22 and AC-5 correspond to Unit T5, and SC-6 and SC-141 (A and B are consecutive sections of the same specimen) correspond to Unit T6. Thicknesses and luminance time series values were measured along Path-A (black) and Path-B (red).

Figure 3. A) Lamina shape based on Preiss (1972, 1976) and Walter (1972), in Kennard and Burne (1989). B) Types of laminae based on textural differences, simplified from Martin-Bello et al. (2019b). C) Thin section and (D) polished section of quasi equivalent, mirror planes of a micritic stromatolite in the study area. DCL: dark composite laminae; LCL: light composite laminae.

Figure 4. A) Bulk isotopic analyses of C and O performed across specimen PL-22 in light (l) and dark (d) laminae. B) High-resolution sampling in PL-22t 7l and PL-22t 8d, and orders of cyclicity according to Martin-Bello et al. (2019a).

Figure 5. Stromatolite laminae arrangement, showing the annual (A) and multi-annual nature (B) of lamination, based on Martin-Bello et al. (2019b).

Figure 6. Example of a stromatolite polished section, and identification of the different patterns of cyclicity recognised (SC-6): blue lines correspond to second order cycles according to Martin-Bello et al. (2019a), which in this work are identified with NAO/ENSO-like cycles; red lines correspond to first order cycles after Martin-Bello et al. (2019a), identified with 11-year Schwabe cycles; black lines correspond to supra-order cycles that could be identified with AMO-like cycles.

Figure 7. Example of a stromatolite polished section, and identification of the different patterns of cyclicity recognised (PL-22): blue lines correspond to second order cycles after Martin-Bello et al. (2019a), which in this work are identified with NAO/ENSO-like cycles; red lines correspond to first order cycles after Martin-Bello et al. (2019a), identified with 11-year Schwabe cycles; black lines correspond to supra-order cycles which could be identified with AMO-like cycles.

Figure 8. Spectral analysis results. A to D) Comparison between different singular spectra obtained from SC-6 thickness values based on (A) light laminae, (B) dark laminae, (C) light-dark lamina couplet from Path-A, and (D) light-dark lamina couplet from Path-B. E to H) Singular spectra based on thicknesses of light-dark lamina couplets: E) PL-22 light-dark, F) VS-22 light-dark, G) AC-5 light-dark, and H) SC-141 light-dark. I to L) Singular spectra based on dark lamina thickness values: I) PL-22 dark, J) VS-22 dark, K) AC-5 dark, and L) SC-141 dark. Coloured areas limit the most typical climatic signature frequencies: QBO, Quasi-Biennial Oscillation; ENSO, El Niño-Southern Oscillation; NAO, North Atlantic Oscillation; SUN, Schwabe and Hale sunspot cycles. Time series data are provided in Supplementary material 1.

Figure 9. Continuous wavelet spectra from thicknesses of light-dark lamina couplets performed on Path-A. Time series data are provided in Supplementary material 1. The vertical axis indicates cyclicity periods (years) on a logarithmic scale; the horizontal axis represents

counting of lamina couplets through time (years). The 95% confidence levels are given as thick contour lines.

Table 1. Lacustrine stromatolite growth rates considering annual couplet duration. Capital letters A and B are referred to the path through which the growth rate was calculated (see Fig. 4). * is the combination of SC-141A and SC-141B specimens.

Specimen	Thickness (mm)	Time (years)	Growth rate (mm/yr)	Units
SC-141A*	113.38	531	0.214	T6
SC-6B	36.84	162	0.227	T6
SC-6A	27.70	139	0.199	T6
PL-22A	50.37	118	0.427	T5
PL-22B	67.98	126	0.540	T5
VS-22A	63.98	137	0.467	T5
VS-22B	54.12	106	0.511	T5
AC-5A	59.45	189	0.315	T5
		Average	**0.362**	

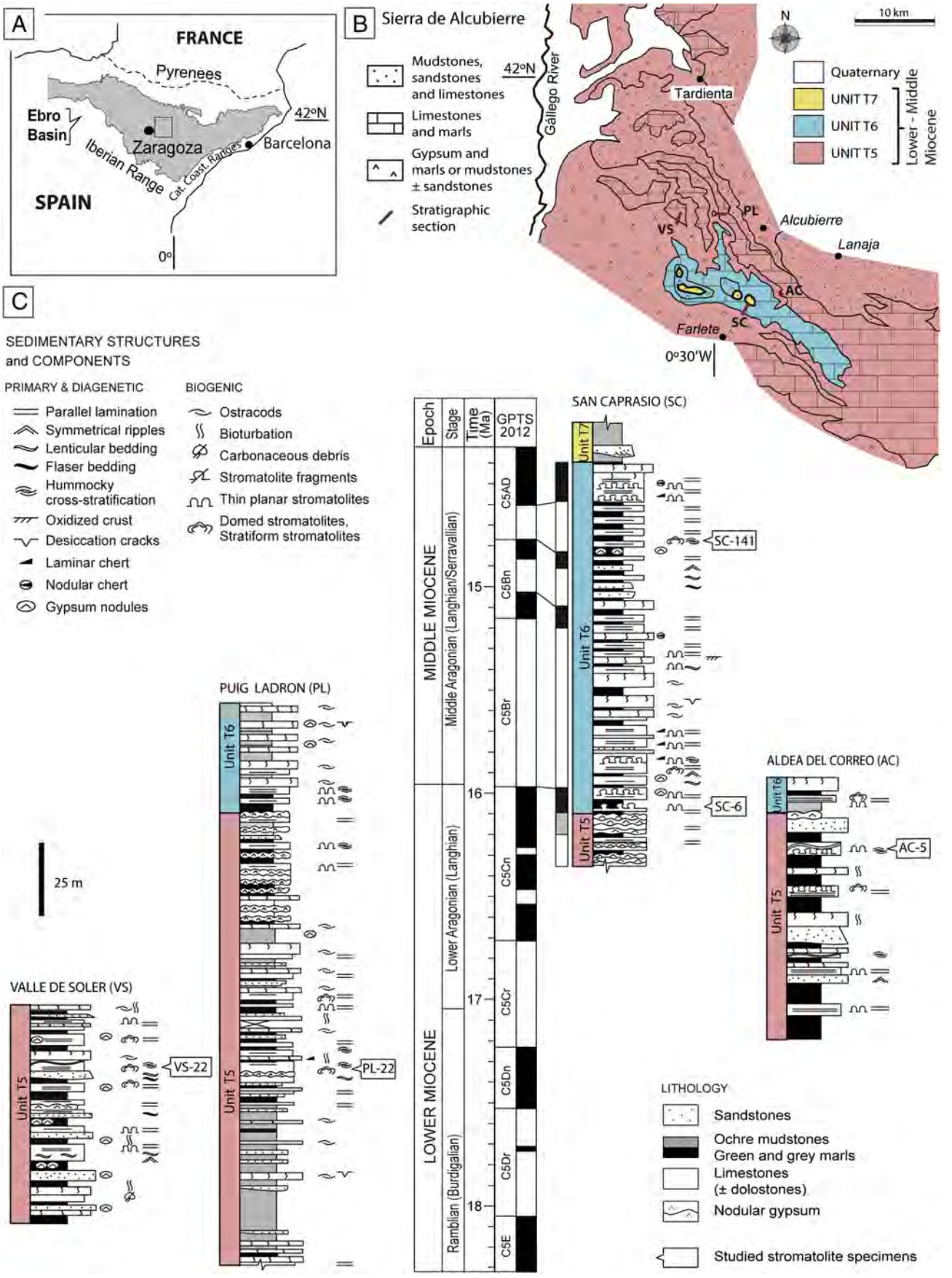
A
FRANCE
Pyrenees
Ebro Basin
Zaragoza
Barcelona
42ºN
Iberian Range
Cat. Coast. Ranges
SPAIN
0º
B
Sierra de Alcubierre
Mudstones, sandstones and limestones
Limestones and marls
Gypsum and marls or mudstones ± sandstones
Stratigraphic section
42ºN
Gállego River
Tardienta
N
10 km
Quaternary
UNIT T7
UNIT T6
UNIT T5
Lower - Middle Miocene
PL
VS
Alcubierre
Lanaja
AC
SC
Farlete
0º30'W
C
SEDIMENTARY STRUCTURES and COMPONENTS
PRIMARY & DIAGENETIC
Parallel lamination
Symmetrical ripples
Lenticular bedding
Flaser bedding
Hummocky cross-stratification
Oxidized crust
Desiccation cracks
Laminar chert
Nodular chert
Gypsum nodules
BIOGENIC
Ostracods
Bioturbation
Carbonaceous debris
Stromatolite fragments
Thin planar stromatolites
Domed stromatolites, Strati form stromatolites
Epoch
Stage
Time (Ma)
GPTS 2012
MIDDLE MIOCENE
LOWER MIOCENE
Middle Aragonian (Langhian/Serravalian)
Lower Aragonian (Langhian)
Ramblian (Burdigalian)
C5AD
C5Bn
C5Br
C5Cn
C5Cr
C5Dn
C5Dr
C5E
15
16
17
18
SAN CAPRASIO (SC)
Unit T7
Unit T6
Unit T5
SC-141
SC-6
PUIG LADRON (PL)
PL-22
VALLE DE SOLER (VS)
VS-22
ALDEA DEL CORREO (AC)
AC-5
25 m
LITHOLOGY
Sandstones
Ochre mudstones
Green and grey marls
Limestones (± dolostones)
Nodular gypsum
Studied stromatolite specimens

Figure 1

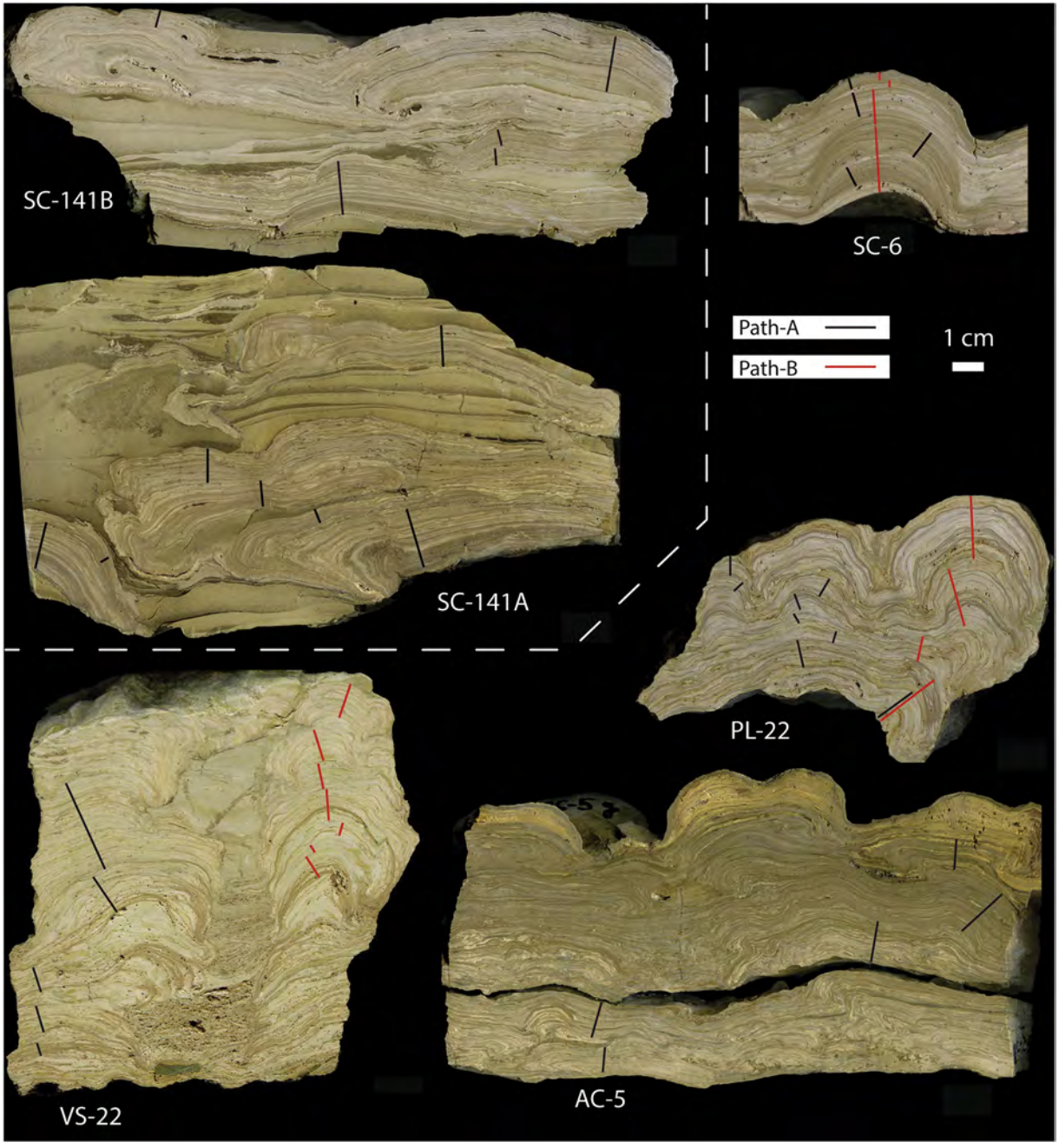

Figure 2

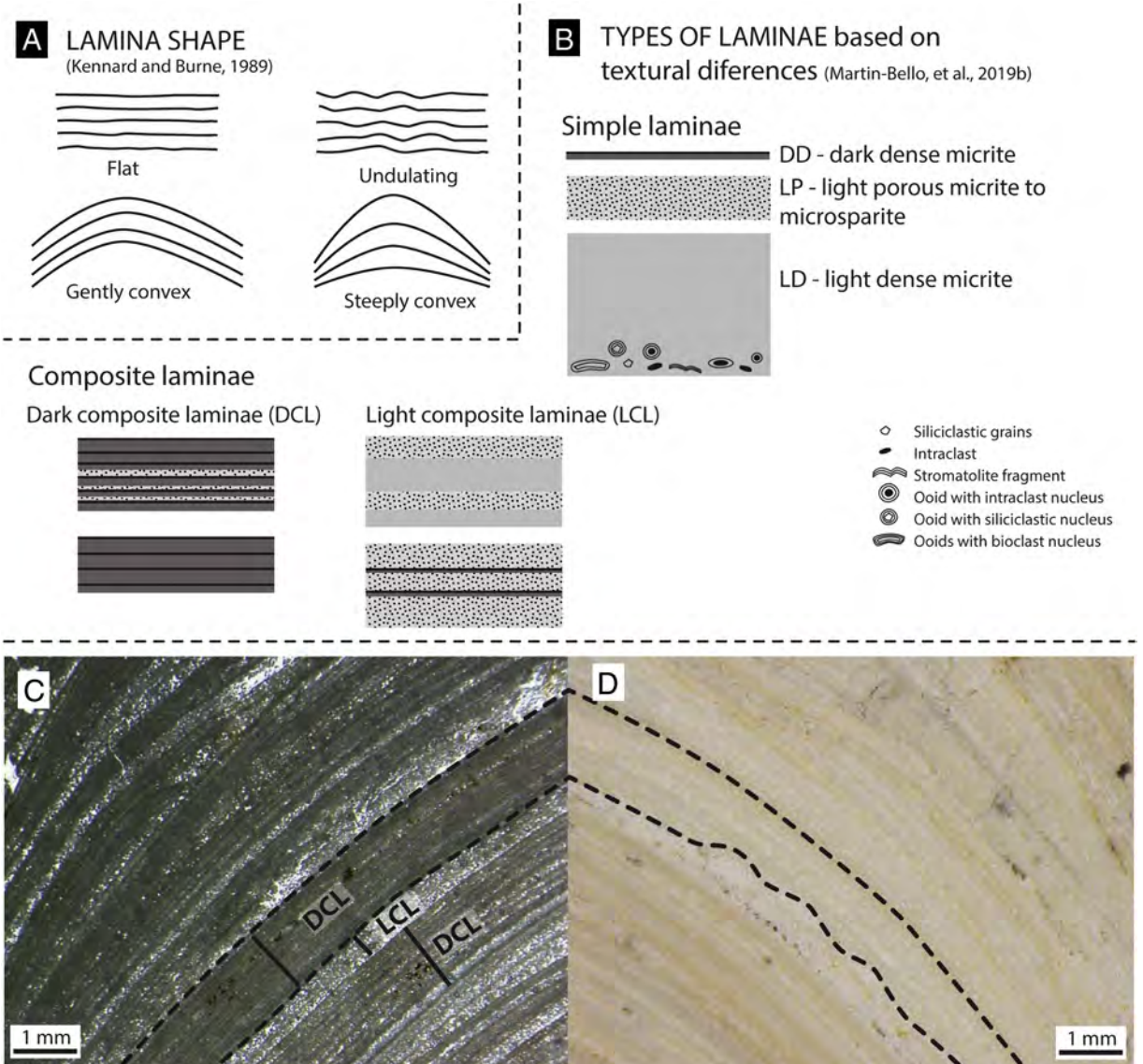
A
LAMINA SHAPE
(Kennard and Burne, 1989)
Flat
Undulating
Gently convex
Steeply convex
B
TYPES OF LAMINAE based on textural diferences (Martin-Bello, et al., 2019b)
Simple laminae
DD - dark dense micrite
LP - light porous micrite to microsparite
LD - light dense micrite
Composite laminae
Dark composite laminae (DCL)
Light composite laminae (LCL)
Siliciclastic grains
Intraclast
Stromatolite fragment
Ooid with intraclast nucleus
Ooid with siliciclastic nucleus
Ooids with bioclast nucleus
C
DCL
LCL
DCL
1 mm
D
1 mm

Figure 3

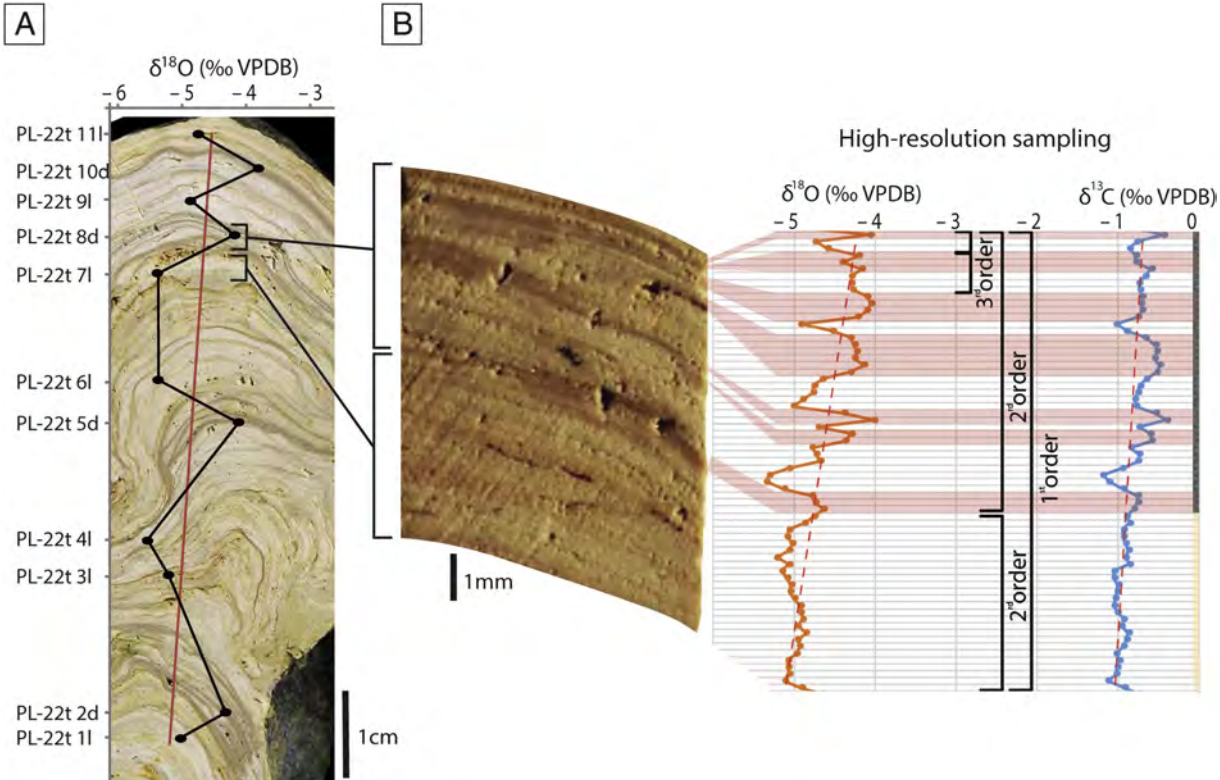
A
B
δ18O (‰ VPDB)
−6
−5
−4
−3
PL-22t 11l
PL-22t 10d
PL-22t 9l
PL-22t 8d
PL-22t 7l
PL-22t 6l
PL-22t 5d
PL-22t 4l
PL-22t 3l
PL-22t 2d
PL-22t 1l
1cm
1mm
High-resolution sampling
δ18O (‰ VPDB)
−5
−4
−3
−2
δ13C (‰ VPDB)
−1
0
3rd order
2nd order
1st order
2nd order

Figure 4

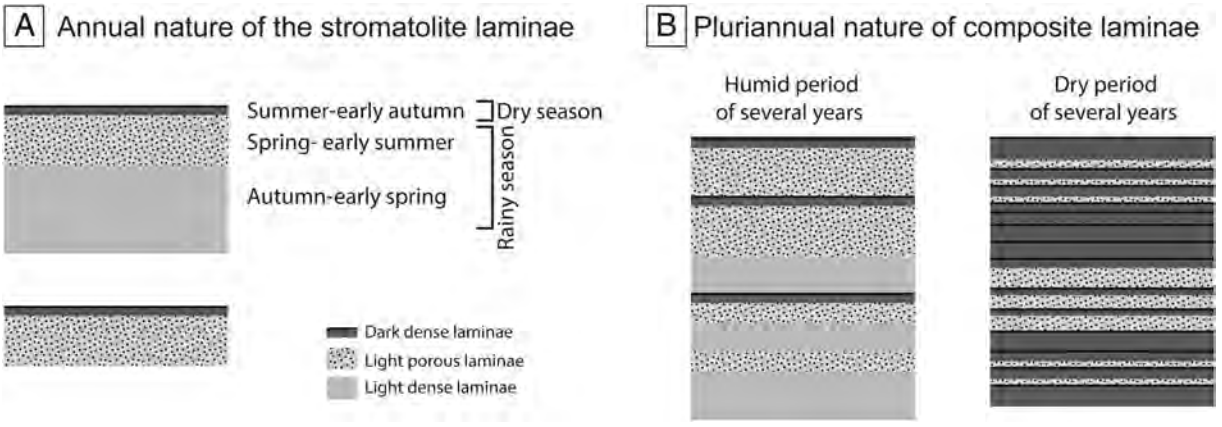
A Annual nature of the stromatolite laminae
Summer-early autumn
Spring- early summer
Autumn-early spring
Dry season
Rainy season
Dark dense laminae
Light porous laminae
Light dense laminae
B Pluriannual nature of composite laminae
Humid period of several years
Dry period of several years

Figure 5

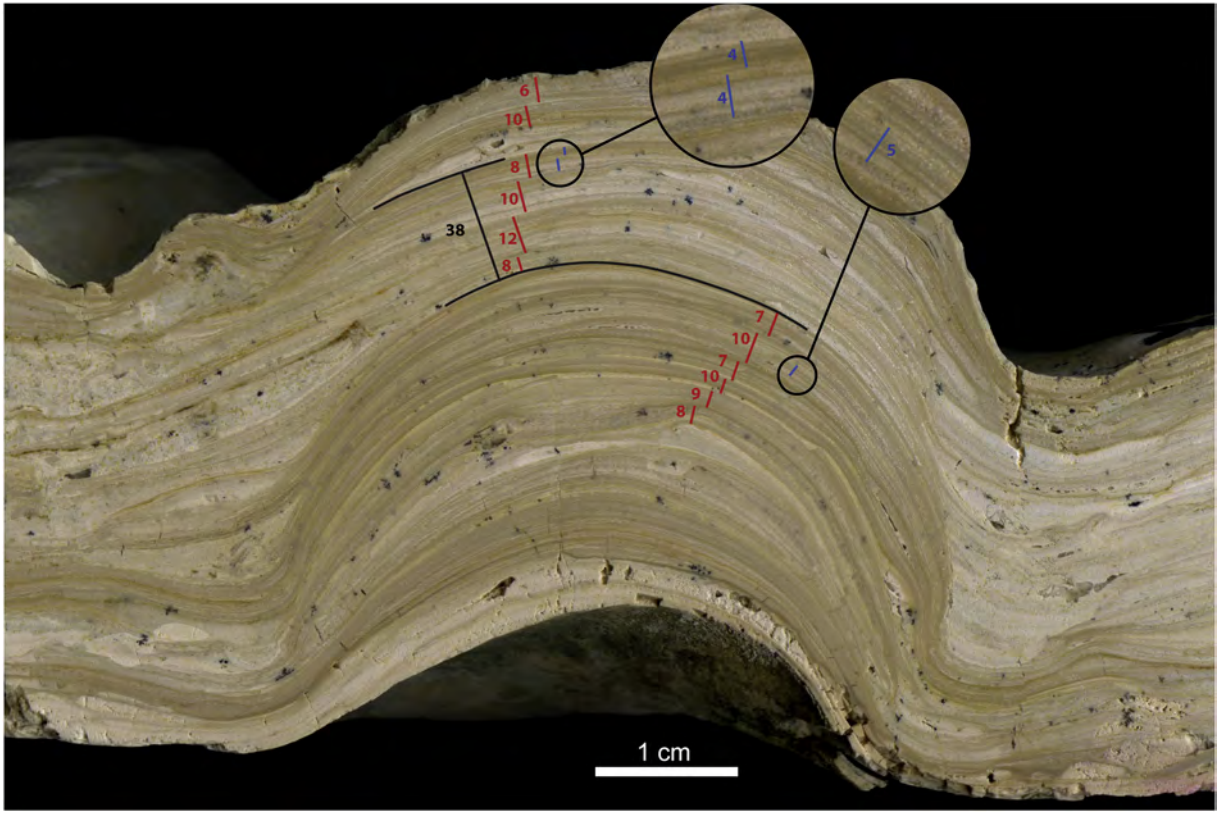

Figure 6

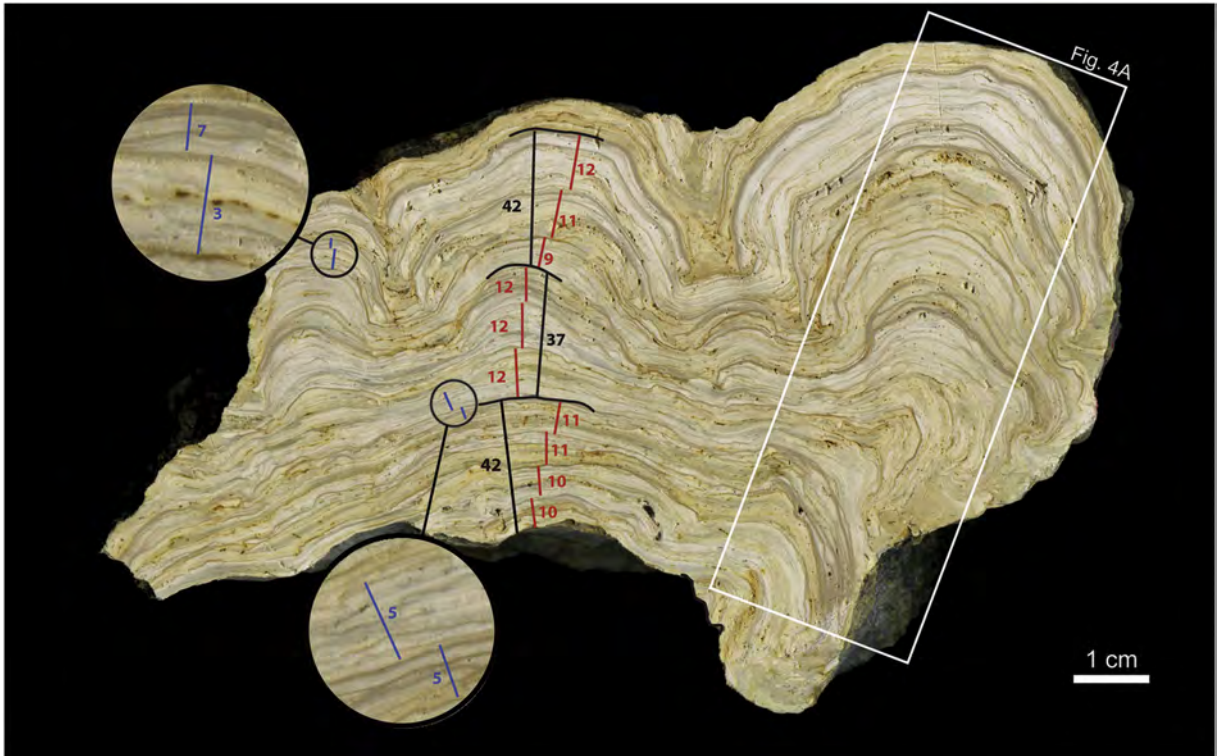

Figure 7

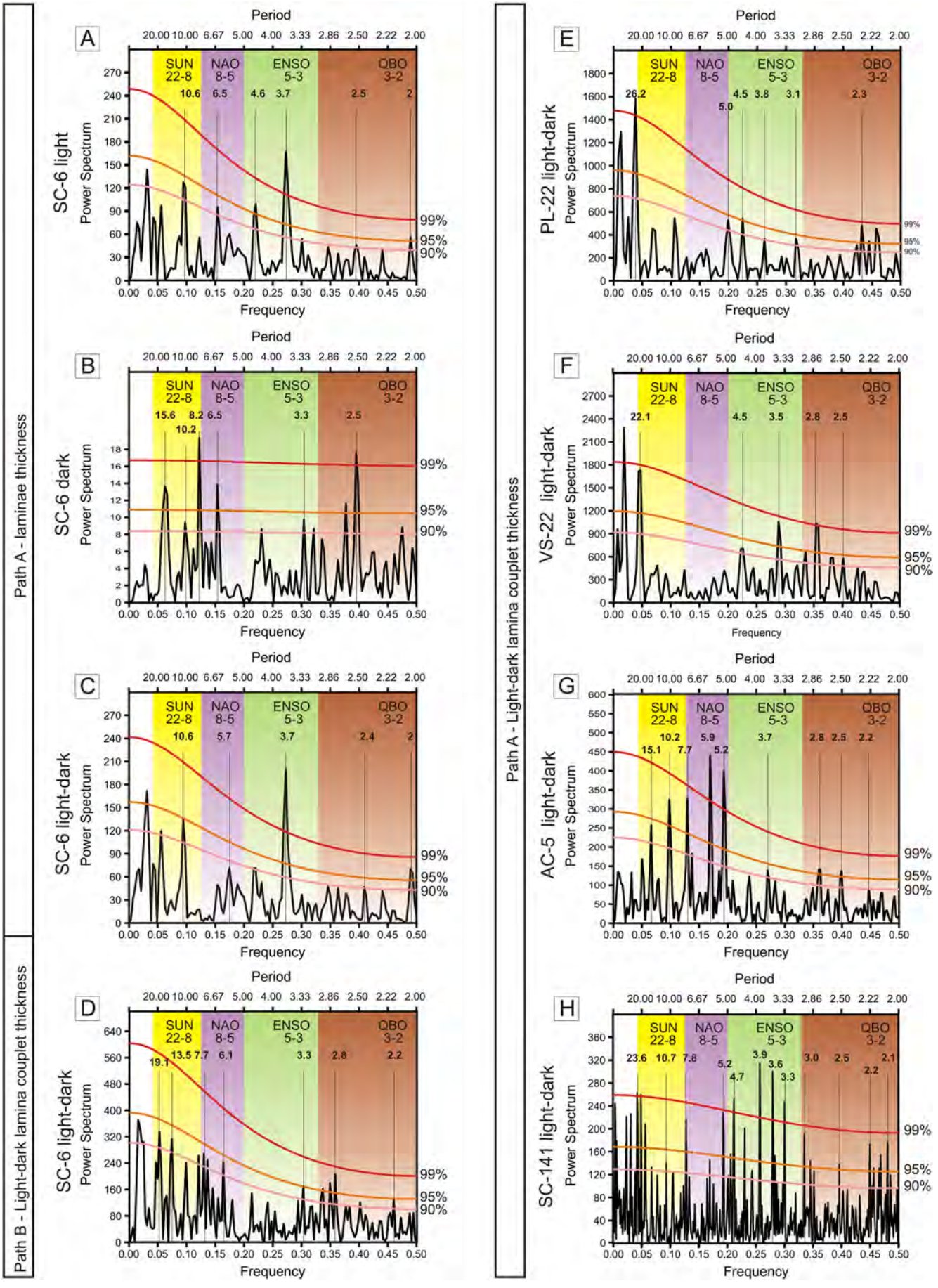
Path A - laminae thickness
Path B - Light-dark lamina couplet thickness
Path A - Light-dark lamina couplet thickness
A
B
C
D
E
F
G
H
SC-6 light
SC-6 dark
SC-6 light-dark
SC-6 light-dark
PL-22 light-dark
VS-22 light-dark
AC-5 light-dark
SC-141 light-dark
Power Spectrum
Period
Frequency
SUN 22-8
NAO 8-5
ENSO 5-3
QBO 3-2
99%
95%
90%

Figure 8r1

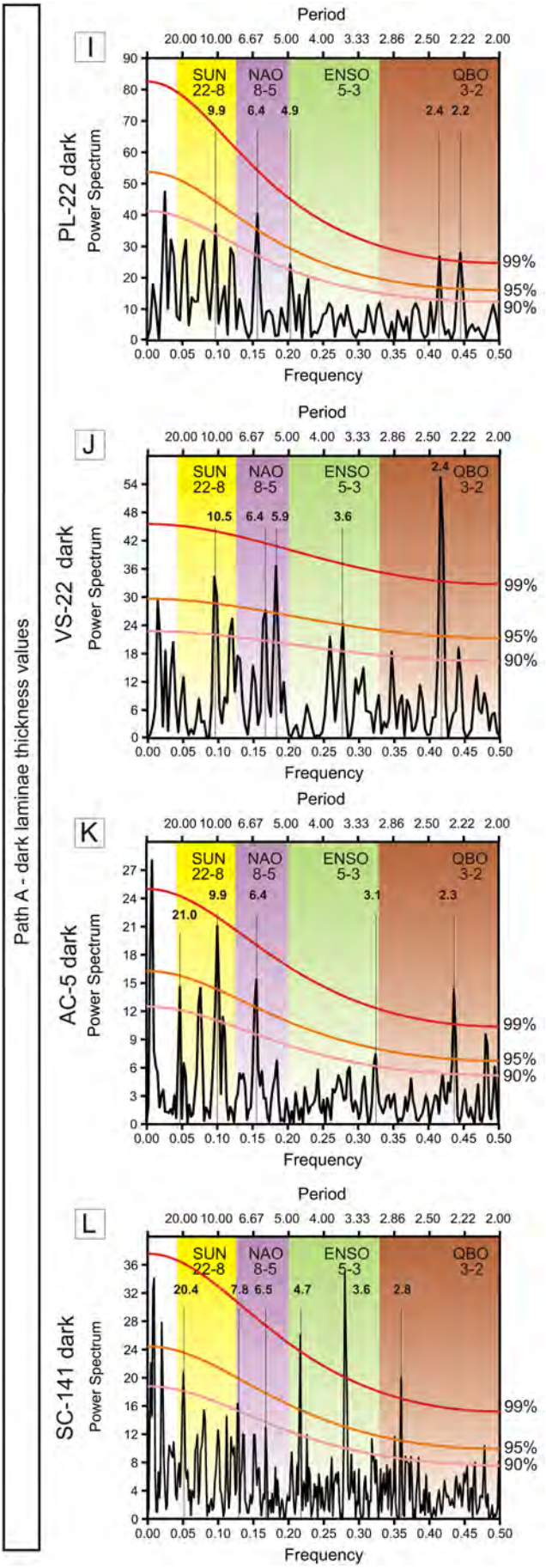
Path A - dark laminae thickness values
I
PL-22 dark
Power Spectrum
Period
20.00 10.00 6.67 5.00 4.00 3.33 2.86 2.50 2.22 2.00
SUN 22-8
NAO 8-5
ENSO 5-3
QBO 3-2
9.9
6.4
4.9
2.4
2.2
99%
95%
90%
Frequency
J
VS-22 dark
Power Spectrum
10.5
6.4
5.9
3.6
2.4
K
AC-5 dark
Power Spectrum
21.0
9.9
6.4
3.1
2.3
L
SC-141 dark
Power Spectrum
20.4
7.8
6.5
4.7
3.6
2.8

Figure 8r2

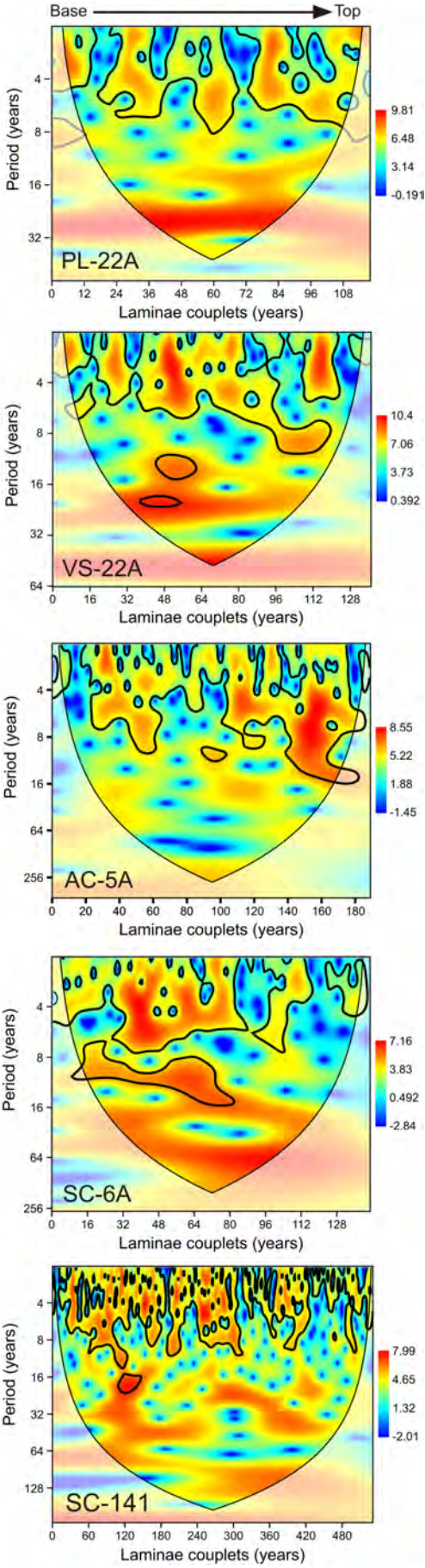
Base
Top
Period (years)
4
8
16
32
9.81
6.48
3.14
-0.191
PL-22A
0 12 24 36 48 60 72 84 96 108
Laminae couplets (years)
Period (years)
4
8
16
32
64
10.4
7.06
3.73
0.392
VS-22A
0 16 32 48 64 80 96 112 128
Laminae couplets (years)
Period (years)
4
8
16
64
256
8.55
5.22
1.88
-1.45
AC-5A
0 20 40 60 80 100 120 140 160 180
Laminae couplets (years)
Period (years)
4
8
16
64
256
7.16
3.83
0.492
-2.84
SC-6A
0 16 32 48 64 80 96 112 128
Laminae couplets (years)
Period (years)
4
8
16
32
64
128
7.99
4.65
1.32
-2.01
SC-141
0 60 120 180 240 300 360 420 480
Laminae couplets (years)

Figure 9